**Muon Ionisation Cooling Experiment**

arXiv:1005.3491v2 [physics.ins-det] 11 Jul 2010

# The design, construction and performance of the MICE scintillating fibre trackers

## Abstract

Charged-particle tracking in the international Muon Ionisation Cooling Experiment (MICE) will be performed using two solenoidal spectrometers, each instrumented with a tracking detector based on 350 $\mu$m diameter scintillating fibres. The design and construction of the trackers is described along with the quality-assurance procedures, photon-detection system, readout electronics, reconstruction and simulation software and the data-acquisition system. Finally, the performance of the MICE tracker, determined using cosmic rays, is presented.

M. Ellis, P.R. Hobson, P. Kyberd, J.J. Nebrensky
*Brunel University, Uxbridge, Middlesex, UB8 3PH, UK*

A. Bross, J. Fagan, T. Fitzpatrick, R. Flores, R. Kubinski, J. Krider, R. Rucinski, P. Rubinov, C. Tolian
*Fermilab, P.O. Box 500, Batavia, IL 60510-0500, USA*

T.L. Hart[1], D.M. Kaplan, W. Luebke, B. Freemire, M. Wojcik
*Physics Division, Illinois Institute of Technology, 3101 S. Dearborn St., Chicago, IL 60616, USA*

G. Barber, D. Clark, I. Clark, P.J. Dornan, A. Fish, S. Greenwood, R. Hare, A. Jamdagni, V. Kasey, M. Khaleeq, J. Leaver, K.R. Long, E. McKigney[2], T. Matsushita[3], C. Rogers[4], T. Sashalmi, P. Savage, M. Takahashi[5], A. Tapper
*Department of Physics, Blackett Laboratory, Imperial College London, Exhibition Road, London SW7 2AZ, UK*

K. Yoshimura
*High Energy Accelerator Research Organization (KEK), Institute of Particle and Nuclear Studies, Tsukuba, Ibaraki, Japan*

P. Cooke, R. Gamet
*Department of Physics, Oliver Lodge Laboratory, University of Liverpool, Liverpool, L69 7ZE, UK*

H. Sakamoto, Y. Kuno, A. Sato, T. Yano, M. Yoshida
*Graduate School of Science, Department of Physics, Osaka University, Toyonaka, Osaka, Japan*

C. MacWaters
*STFC Rutherford Appleton Laboratory, Chilton, Didcot, Oxfordshire, OX11 0QX, UK*

L. Coney, G. Hanson, A. Klier[6]
*University of California, Riverside, Riverside, CA 92521-0413 USA*

D. Cline, X. Yang
*University of California at Los Angeles Physics Department, Los Angeles, CA 90024, USA*

D. Adey
*Department of Physics, University of Warwick, Coventry, CV4 7AL, UK*

---

[1] Now at University of Mississippi, Oxford, MS 38677, USA

[2] Now at Los Alamos Natl. Lab., P.O. Box 1663, Los Alamos, NM 87545, USA

[3] Now at Kobe University, Faculty of Science, 1-1 Rokkodai-cho, Nada-ku, Kobe-shi, Hyogo 657-8501, Japan

[4] Now at STFC Rutherford Appleton Laboratory, Chilton, Didcot, Oxon, OX11 0QX, UK

[5] Now at the University of Manchester, School of Physics and Astronomy, Schuster Laboratory, Manchester M13 9PL, UK

[6] Now at Weizmann Institute of Science, Department of Particle Physics, P.O. Box 26, Rehovot 76100, Israel

# Contents

# 1 Introduction

Muon storage rings have been proposed for use as sources of intense high-energy neutrino beams in a Neutrino Factory [1] and as the basis for multi-TeV lepton-antilepton colliding-beam facilities [2]. To optimise the performance of such facilities requires the phase-space compression (cooling) of the muon beam prior to acceleration and storage. The short muon-lifetime makes it impossible to employ traditional techniques to cool the beam while maintaining the muon-beam intensity. Ionisation cooling, a process in which the muon beam is passed through a series of liquid hydrogen absorbers interspersed with accelerating RF cavities, is the technique proposed to cool the muon beam. The international Muon Ionisation Cooling Experiment (MICE) will provide an engineering demonstration of the ionisation-cooling technique and will allow the factors affecting the performance of ionisation-cooling channels to be investigated in detail [3]. Muon beams of momenta between 140 MeV/c and 240 MeV/c, with normalised emittances between 2 $\pi$mm and 10 $\pi$mm, will be provided by a purpose-built beam line on the 800 MeV proton synchrotron, ISIS [4], at the Rutherford Appleton Laboratory [5].

MICE is a single-particle experiment in which the position and momentum of each muon is measured before it enters the MICE cooling channel and once again after it has left (see figure 1) [6]. The MICE cooling channel, which is based on one lattice cell of the cooling channel described in [7], comprises three 20 $l$ volumes of liquid hydrogen and two sets of four 201 MHz accelerating cavities. Beam transport is achieved by means of a series of superconducting solenoids. A particle-identification (PID) system (scintillator time-of-flight hodoscopes TOF0 and TOF1 and threshold Cherenkov counters CKOVa and CKOVb) upstream of the cooling channel allows a pure muon beam to be selected. Downstream of the cooling channel, a final hodoscope (TOF2) and a calorimeter system allow muon decays to be identified. The calorimeter is composed of a KLOE-like lead-scintillator section (KL) followed by a fully active scintillator detector (the electron-muon ranger, EMR) in which the muons are brought to rest. For a full description of the experiment see [6].

Charged-particle tracking in MICE is provided by two solenoidal spectrometers. Together, the spectrometers are required to determine the expected relative change in transverse emittance of approximately 10% with a precision of $\pm1\%$ (i.e. a 0.1% measurement of the absolute emittance). The trackers themselves are required to have high track-finding efficiency in the presence of background induced by X-rays produced in the RF cavities. Each spectrometer consists of a 4 T superconducting solenoid of 40 cm bore instrumented with a tracker composed of five planar scintillating-fibre stations. Each station is composed of three doublet-layers of scintillating fibres laid out in a '$u, v, w$' arrangement. To reduce multiple Coulomb scattering of muons to an acceptable level, a fibre diameter of 350 $\mu$m is required. The scintillation light is read out via 1.05 mm clear-fibre light-guides. To reduce the cost of the readout electronics seven 350 $\mu$m fibres are read out through each clear-fibre light-guide. The active area of each station is a circle of diameter 30 cm.

The concentration of the primary and secondary dopants within the scintillating fibre must be chosen to maximise the light yield while minimising the fibre-to-fibre optical cross talk. The
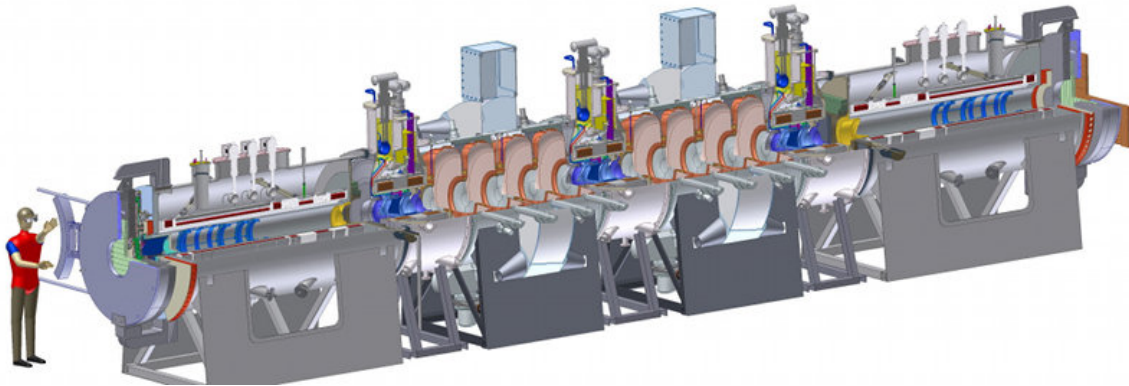
Figure 1: Cutaway 3D rendering of the international Muon Ionisation Cooling Experiment (MICE). The muon beam enters from the bottom left of the figure. The upstream PID instrumentation (not shown) is composed of two time-of-flight hodoscopes (TOF0 and TOF1) and two threshold Cherenkov counters (CKOVa and CKOVb). The upstream spectrometer is followed by the MICE cooling channel, which is composed of three 20 $l$ volumes of liquid hydrogen and two sets of four 201 MHz accelerating cavities embedded in a solenoidal transport channel. This in turn is followed by the downstream spectrometer, a third time-of-flight hodoscope (TOF2), and a calorimeter system (KL and EMR).

passage of a charged particle through the fibre causes energy to be transferred to the primary dopant, para-terphenyl (pT). The peak of the scintillation light spectrum of pT is at a wavelength of $\sim 350$ nm [8]. The secondary dopant, 3-hydroxflavone (3HF), absorbs this light and re-emits it at a wavelength of $\sim 525$ nm [9]. The concentration of primary dopant must be such that efficient energy transfer from the polymer to the pT occurs. The energy-transfer process, known as the Förster Transfer [10] process, occurs when the mean distance between a polymer molecule and a pT molecule is on the order of 10 angstroms. It is this criterion that determines the minimum concentration required for efficient transfer. The concentration of 3HF must be small enough to ensure negligible secondary light attenuation along the length of the active fibre, but large enough that the absorption length of the primary light in the 3HF is small compared to the fibre diameter. The latter condition ensures that fibre-to-fibre cross talk is eliminated. Light-yield measurements using prototype stations led to the choice of 1.25% and 0.25% by weight for the concentrations of pT and 3HF respectively [11]. Light with wavelength shorter than around 450 nm damages the secondary dopant (3HF) and causes discolouration of the fibres and therefore reduces the light yield. For this reason, filtered light was used throughout the fabrication process and steps in the process were photographed without the use of flash.

The MICE trackers are read out using the DØ Central Fiber Tracker (CFT) optical readout and electronics system [12]. The scintillation light is detected using Visible Light Photon Counters (VLPCs) [13, 14]. These are low band-gap silicon avalanche devices that are operated at 9 K. The VLPCs have a high quantum efficiency ($\sim 80\%$) and a high gain that in some devices is in excess of 50 000. The VLPC signals are digitised using the Analogue Front End with Timing (AFE IIt) board developed by the DØ collaboration [15].

The solenoidal field in the tracking volume is designed to be uniform at the 3 per mil level. The MICE coordinate system is such that the $z$ axis is parallel to the beam, the $y$ axis points
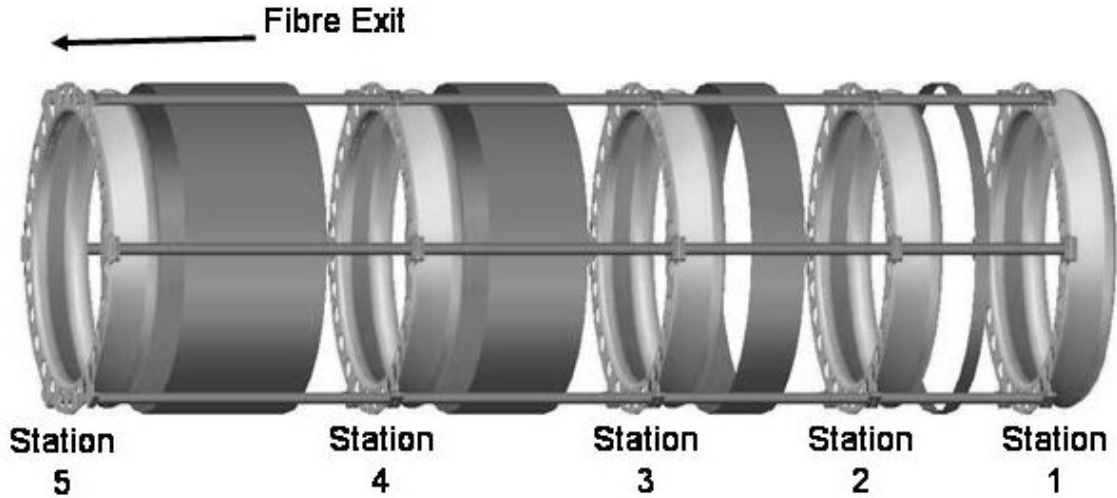
2

Figure 2: Schematic diagram of the MICE tracker. The five stations are shown supported by the carbon-fibre space frame, with fibres omitted for clarity. The station numbering scheme is indicated together with the direction in which the clear-fibre light-guides leave the tracking volume.

vertically upwards, and the $x$ axis completes a right-handed coordinate system. A muon therefore describes a circle in the $x, y$ plane as it travels through the solenoid. The transverse momentum of the muon is obtained by determining the radius of this circle, while the number of turns determines the $z$-component. The station spacing has been chosen to optimise the performance of the reconstruction (track-finding efficiency and parameter resolution).

This paper is organised as follows. The mechanical design and construction of the trackers are described in section 2. The photon-detection system and readout electronics are presented in sections 3 and 4 respectively. Section 5 contains a summary of the performance of the devices. Finally, a summary is presented in section 6.

## 2    Mechanical design and construction

The layout of the MICE tracker is shown in figure 2. The five stations are held in position using a carbon-fibre space-frame. The distance between neighbouring stations is such that each nearest-neighbour spacing is unique. This ensures that the azimuthal rotation of track position from one station to the next differs, this difference being important in resolving ambiguities at the pattern-recognition stage. The station spacing, together with other key parameters of the tracker module, are presented in table 1.

Each station consists of three 'doublet layers' of 350 $\mu$m scintillating fibres glued on a carbon-fibre station body. The doublet layers are arranged such that the fibres in one layer run at an angle of 120° to the fibres in each of the other layers as shown in figure 3a. The arrangement

3

Table 1: Key parameters of the MICE tracker module. The first section of the table presents the parameters of the scintillating-fibre tracker itself. The second section reports the environment within the tracking volume in which the tracker must operate. The final section reports the parameters of the MICE spectrometer solenoid that directly affect the performance of the tracker.

| Component | Parameter | Value |
|---|---|---|
| **Scintillating fibre tracker** | Scintillating fibre diameter | 350 $\mu$m |
| | Primary dopant, pT, concentration | 1.25% (by weight) |
| | Secondary dopant, 3HF, concentration | 0.25% (by weight) |
| | Fibre pitch | 427 $\mu$m |
| | Estimated light yield per single fibre | 10 photo-electrons |
| | Number of scintillating fibres per optical readout channel | 7 |
| | Position resolution per plane | 470 $\mu$m |
| | Views per station | 3 |
| | Radiation length per station | 0.45% |
| | Stations per spectrometer | 5 |
| | Station separation: 1 - 2 | 20 cm |
| | Station separation: 2 - 3 | 25 cm |
| | Station separation: 3 - 4 | 30 cm |
| | Station separation: 4 - 5 | 35 cm |
| **Tracking volume** | Sensitive volume: length | 110 cm |
| | Sensitive volume: diameter | 30 cm |
| | Gas in warm bore of spectrometer solenoid | Helium at atmospheric pressure |
| **Spectrometer solenoid** | Magnetic field in tracking volume | 4 T |
| | Field uniformity in tracking volume | 3 per mil |
| | Field stability | 1 per mil |
| | Warm bore diameter | 40 cm |
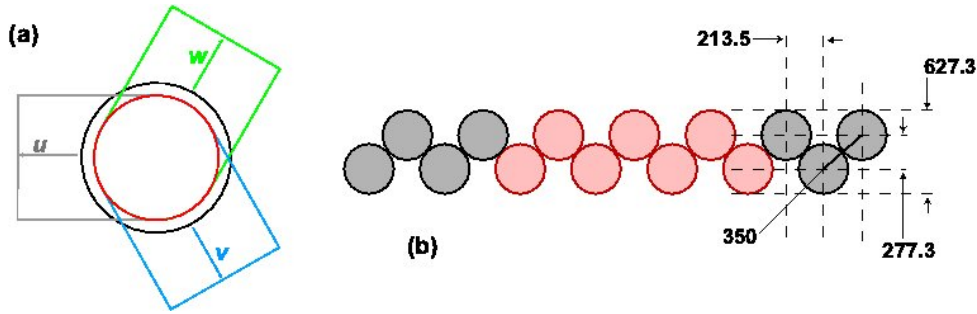
Figure 3: (a) Arrangment of the doublet layers in the scintillating-fibre stations. The outer circle shows the solenoid bore while the inner circle shows the limit of the active area of the tracker. The grey, blue, and green arrows indicate the direction that individual 350 $\mu$m fibres run in the $u, v$, and $w$ planes respectively. (b) Detail of the arrangement of the scintillating fibres in a doublet layer. The fibre spacing and the fibre pitch are indicated on the right-hand end of the figure in $\mu$m. The pattern of seven fibres ganged for readout in a single clear-fibre light-guide is shown in red.

of the fibres within a doublet layer is shown in figure 3b. This packing arrangement ensures that there are no inactive regions between adjacent fibres. The configuration of the seven fibres ganged for readout via a single clear-fibre light-guide is also indicated in figure 3b.

The performance of the tracker is determined by the light yield and the fibre pitch. The seven-fold ganging (see figure 3b), combined with a fibre pitch of 427 $\mu$m (see table 1), yields an expected spatial resolution per doublet layer of 470 $\mu$m. The expected light yield was estimated by extrapolating that obtained in the DØ fibre tracker which used 835 $\mu$m scintillating fibres with similar dopant concentrations [12]. Taking into account the scintillating-fibre diameter used in MICE (350 $\mu$m) and assuming a maximum clear-fibre light-guide length of 4 m, a light yield of $\sim 10$ photo-electrons is obtained [16].

## 2.1 The scintillating-fibre stations

### 2.1.1 Doublet-layer design and fabrication

The design of the doublet layer is shown in figure 4a. A photograph of a completed doublet layer is shown in figure 4b. At this stage in the manufacturing process, the scintillating-fibre planes were referred to as 'ribbons' in view of the length of scintillating fibre extending beyond the active area. The diameter of the circular part of the ribbon, which forms the doublet layer, was 32 cm. This allowed sufficient material for the ribbon to be bonded to the station body.

The scintillating fibre used to make the ribbons was procured in the form of 1 m long canes. The canes were cut to length and then polished so that an aluminium mirror could be applied to one end of the fibre. This was achieved by placing batches of 500 canes in a water-tight former. Water was poured into the former and frozen so that the fibres were supported in a block of ice. The ice/scintillating-fibre structure was then immersed in liquid nitrogen to ensure that the ice was hard. Once cold, the ice/scintillating-fibre structure was polished using a diamond tool.
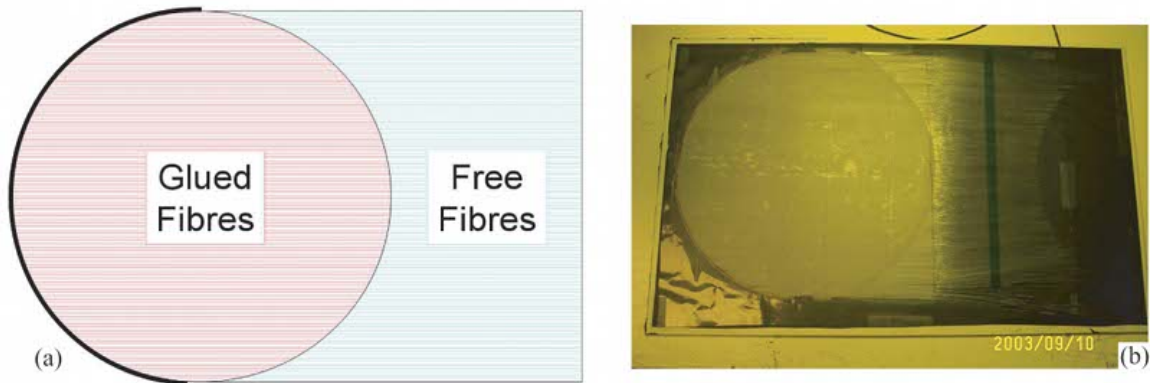
Figure 4: (a) Schematic diagram of the scintillating-fibre ribbon. The circular area of diameter 32 cm that is glued to form the doublet layer is indicated by the red hatching. The mirrored end of the fibre is indicated by the solid black line. (b) A photograph of a completed ribbon on its substrate.
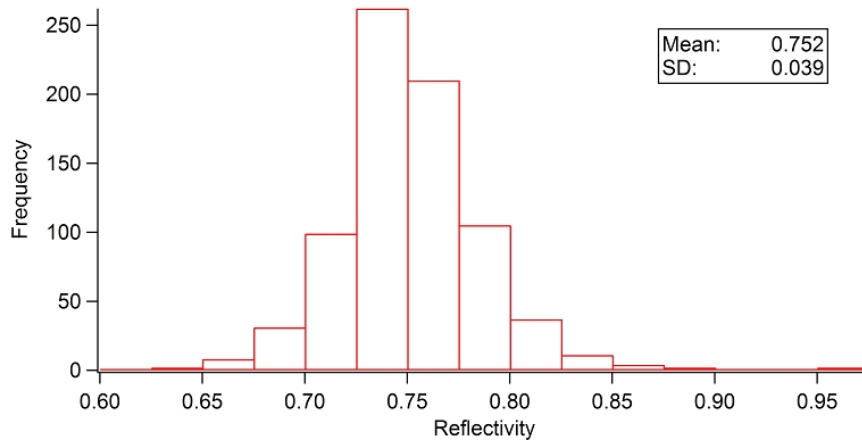


Figure 5: Distribution of reflectivity obtained in the QA measurements on the aluminium mirror formed by vapour deposition on the 350 $\mu$m scintillating fibres used in the construction of the doublet layers. The mean and standard deviation (SD) of the distribution of reflectivities are shown in the inset.

After diamond polishing, the batches of fibre were thawed and an aluminium mirror formed by vapour deposition on the polished end.

A sample of fibres was taken from each of the batches and the reflectivity of the mirrors was determined as follows: a 1 m length of fibre with a mirror on one end was excited using a near-UV LED that excited the 3HF dopant directly. The excitation light was detected with a photo-diode. The output current was measured in this configuration and then the end of the fibre with the mirror was cut off (approximately 5 mm of fibre was removed). This end was then painted black (to kill any possible reflection from this end) and then the LED test was repeated. The ratio of the signal with the mirror to that without mirror is equal to $1 + R$, where R is the relectivity of the mirror. The results of the measurements are shown in figure 5. The average reflectivity of the mirrors used in the MICE trackers is 75% and the standard deviation of the reflectivity distribution is approximately 4%.

6

Scintillating-fibre ribbons were made following the technique developed for the DØ fibre tracker [12]. A grooved mould was machined in Delrin. The mould was measured on a coordinate measuring machine and the mean groove pitch was determined to be 427 $\mu$m. Holes were drilled into the grooves to allow air to be pumped away from the spaces within the grooves. A Teflon release film, of thickness 25 $\mu$m, was pressed into the mould with the aid of a vacuum established via the holes mentioned above. A 'tack' adhesive was then sprayed on the Teflon and the first layer of scintillating fibres was placed in the grooves. A circular stop, machined from a plastic sheet, was placed over the mould so that, by butting the mirrored end of the fibre canes against the stop, a ribbon with the proper circular active area could be formed. After the first layer of fibre was in the mould, spray adhesive was applied to the fibre and the second layer of fibre (forming the doublet layer) was placed on top of the first layer, offset by half a fibre width. A polyurethane adhesive was then spread over the fibres and a 25 $\mu$m Mylar film was placed over the whole assembly. The assembly was then clamped to apply a uniform pressure over the doublet layer for a period of at least 12 hours to allow the adhesive to cure. The resultant 'ribbon' was removed from the mould with the release film still attached. The final step in the ribbon fabrication was to remove carefully the release film from the ribbon.

### 2.1.2 Station body

The station body was fabricated in carbon fibre 'prepreg' (pre-impregnated with resin) supplied by the Advanced Composites Group (UK). The fibre specification was CF1300, 150 g/m$^2$, 2 × 2 Twill Weave 1K HS and was impregnated with 45% by weight VTM264 resin. The station body was produced in the form of a low-mass shell capable of supporting the scintillating fibres, with a flange for optical connectors and for attachment to the space frame (see figure 6a). The external diameter of the flange is 40 cm with the flat scintillating-fibre contact area having an inner diameter of 30 cm and an outer diameter of 32 cm. A radius was formed to ensure that the fibres would not be bent by more than the minimum bend radius as they passed from the active surface to the optical connectors on the flange. The overall depth of the station is 65 mm.

A two-part female mould tool was manufactured in aluminium to the required shape. The tool was doweled and bolted together to ensure accuracy. The surface was polished to a high gloss and degreased. A release coating of wax was applied to the mould each time it was used. Due to the complex nature of the shape and the difficulty of laying-up the carbon fibre, it was necessary to divide the station body into 12 identical 30$^o$ azimuthal segments. A template was produced and enough parts were cut to provide three overlapping layers (36 pieces). The first layer was built up on the tool from 12 segments. Each subsequent layer was then layed with the segments offset azimuthally by 10$^o$ from the previous layer. To build up the flange area in preparation for a subsequent machining process, 7 ring-shaped layers were also applied to the tool.

Once all the carbon fibre pieces were present in the layup, the assembly had layers of release and breather film applied before being sealed in a vacuum bag and placed in an autoclave for

Figure 6: (a) Photograph of a carbon fibre station body after curing in the autoclave. (b) Photograph of the station body after final machining. The holes that take the station connectors and the flanges that mate to the space frame are shown.

cure. The cure cycle used was as follows:

- Apply vacuum to the inside of the bag;

- Raise the temperature to $80^o$ C at a rate of $0.5^o$ C/minute and increase the pressure on the outside of the bag to 90 psi at a rate of 10 psi/minute;

- Hold at $80^o$ C and 90 psi for four hours; and

- Release the external pressure and cool to $20^o$ C before removing the vacuum.

Once cured, the stage was removed from the tool, dressed and made ready for machining. After machining, the approximate final cured thicknesses were: fibre plane and curved sections, 0.55 mm; flange area, 2 mm. The station was then machined on a CNC milling machine. A finished station is shown in figure 6b.

### 2.1.3 Station assembly

The first step in processing the fibre ribbons was to group the individual fibres into the correct seven-fibre bundles. The bundles of seven were held together using black rubber tubes and placed in a comb to allow the first stage of the optical quality-assurance (QA) process to be carried out, as described in the next section. The bundles were then fitted into the station connectors. The rubber tubes helped keep the fibres together as they were inserted into the holes in the connector. The rubber tubes, which can be seen in figure 9, remain on the fibre bundle to add strength and to protect the bundle. When all fibre bundles had been fitted to station connectors a second optical QA procedure was carried out to ensure that the fibres were fitted to the correct hole in the correct connector. Once this had been accomplished, the doublet layers with connectors fitted were aligned onto the vacuum chuck with a precision of $\pm \sim 1$ mm and secured by vacuum. Once the doublet layer had been secured, the chuck was
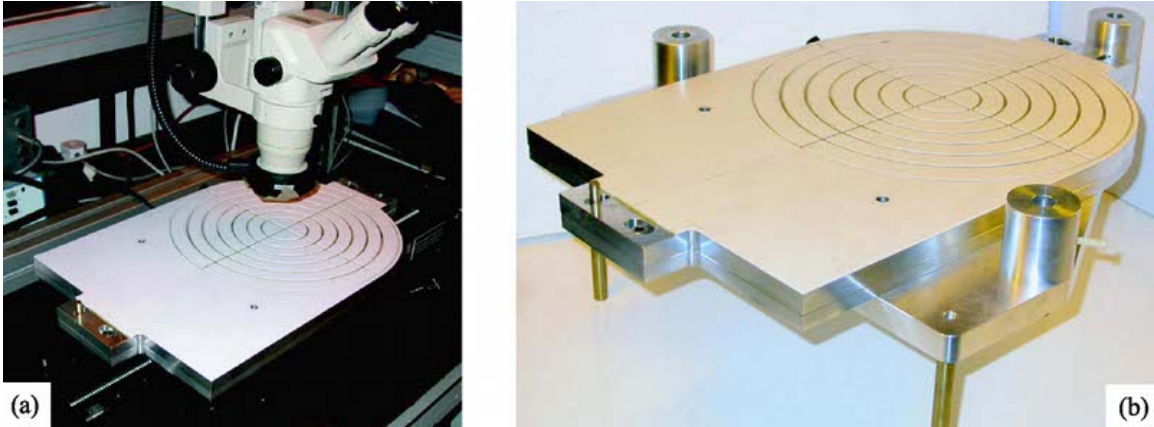
Figure 7: (a) Photograph of the vacuum chuck in position on the linear stage. The circular and diagonal grooves cut in the white Teflon sheet distribute the vacuum across the doublet layer. The photograph also shows the microscope head; and (b) Photograph of the vacuum chuck in position on the gluing jig.
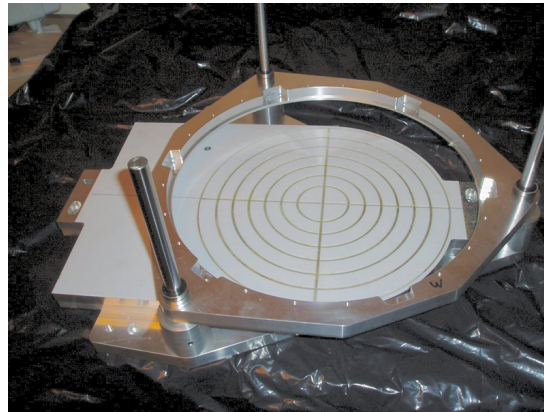


Figure 8: Station holder positioned over vacuum chuck. The photograph shows the station holder in position, located by the three precision dowels located at the vertices of an equilateral triangle.

aligned precisely with respect to three locating dowels using a microscope and linear stage (see figure 7a).

When the alignment was complete, the chuck was locked in position and the dowels were used to locate the vacuum chuck, complete with doublet layer, onto the assembly jig (see figure 7b). The assembly jig had two main parts, the vacuum chuck holder, or base, and the station holder; both of which are shown in figure 8. The station holder, as the name implies, fixed the carbon-fibre station body in the desired location (using dowels) in relation to the three guide shafts. Once the station body was in the holder it remained there until all three doublet layers had been glued in place. The guide shafts were set at 120° azimuthal spacing to give the required azimuthal alignment from doublet layer to doublet layer.

The first doublet layer was glued directly onto the carbon-fibre station body. Once the glue had cured, securing the plane to the station body, the connectors were fitted into their correct positions on the station-body flange. The next doublet layer was laid up on the vacuum chuck,
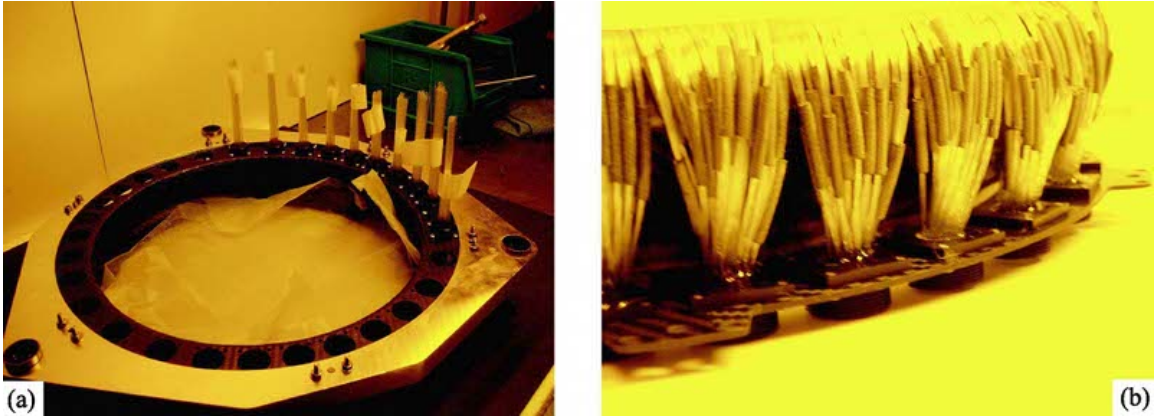
9

Figure 9: (a) Photograph of station clamped in station holder. The first doublet layer has been glued to the station body and the connectors have been fitted to the flange. Adhesive will now be applied to the connector face as described in the text. (b) Photograph showing in detail the fibre run from the doublet layer to the station connector. The station connectors (facing down) have been polished.

aligned as described above, and glued to the first doublet layer. Once the optical connectors serving the second doublet layer had been secured in position, the third doublet layer was glued to the second using the same procedures. Great care was taken to avoid producing trapped air pockets between doublet layers since any such pockets would result in changes in the distance between doublet layers in response to changes in barometric pressure. To accomplish this, the glue was not allowed to form a complete circle around the active area.

When all connectors had been attached to the station body, the fibres were potted into the connectors. To ensure the best possible 'lay', the fibres were gently pulled and eased into position, see figure 9. When the fibres were at the best possible position, without any undue strain, they were potted. To do this the fibres were cut so that approximately 25 mm of fibre protruded from the face of the connector. A vacuum cup was then fitted to the connector and potting adhesive was applied in the recess on the fibre-entry side of the connector. The vacuum applied ensured that the adhesive travelled the length of the fibre within the bore. After the adhesive had been extruded through the bore, the vacuum was removed and the recess 'topped up' with additional adhesive. When the adhesive was in a stable state (i.e. had hardened) the station was turned over and adhesive was applied to the front face of the connector around the fibres to prevent any movement or vibration in subsequent cutting and polishing operations.

Once the glue had cured, excess fibre and cured adhesive was cut at a distance of 2–3 mm from the surface of the connector. The remaining excess material was removed using a diamond-tipped tool. The same tool was also used to skim the surface of the connector to give the required high-quaility finish without the need for further polishing steps which may have degraded the surface flatness. Figure 10 shows a photograph of the fibre bundles after polishing.

### 2.1.4  Station quality assurance procedures
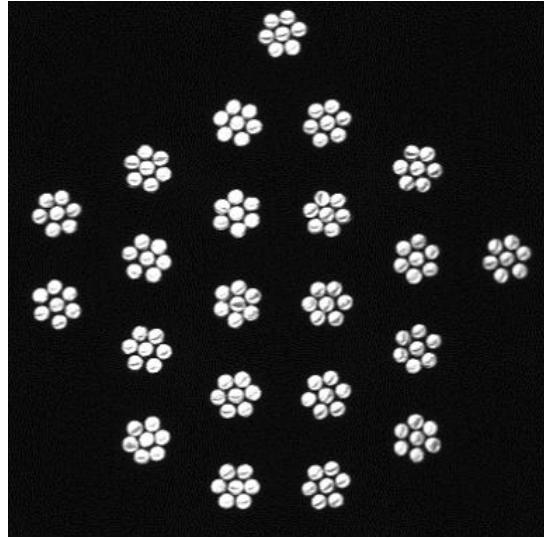
**Optical quality assurance procedures**

Figure 10: Photograph of the face of one station connector. The doublet layer was illuminated with a defocused beam of light so that all fibres were excited. The bundles of seven fibres may clearly be seen.

Each bundle of seven scintillating fibres is expected to produce a signal of approximately equal strength. The QA procedures applied during the station fabrication process exploited this property to identify fibres that were damaged.

*Fibre Doublet Scanning Machine*

A weak 405 nm LED was used to excite the green fluorescent emission of the 3HF dopant in each fibre. Each doublet layer was held on the vacuum chuck which was fitted to a precision stage as described above. The stage was used to step the line-focused LED source over the doublet layer, exciting successive fibres in turn. A sensitive video camera was used to view the end of each bundle of seven fibres. The response of the video camera was recorded and used to measure the transmitted light.

An Anorad WRL-750 linear-motor driven stage, with a total travel of 750 mm and a precision of 10 $\mu$m, carried an optical system to illuminate the fibres. The stage was driven from a PC via an RS232 link to an SB 1091 controller. A CCD-based video camera, Toshiba CS8620Ci, was connected to the PC via a Matrox Meteor II PCI card. The LED, type ETG-5UV405-15, was switched on and off under PC control using one of the eight digital outputs of the SB 1091 controller. The scanning machine is shown schematically in figure 11a while figure 11b shows a photograph of the machine as built.

The LED produces a soft-edged, approximately circular, diverging beam of light (illumination half-angle of 15°), which is projected onto a narrow line by a two-stage optical system [17]. The illumination system is shown schematically in figure 12a. Figure 12b shows a schematic of the rays in the focusing system.

The first stage of the optical system uses cylindrical optics to transform the beam from the LED from a circular to a linear cross-section. As an LED is an extended source and includes
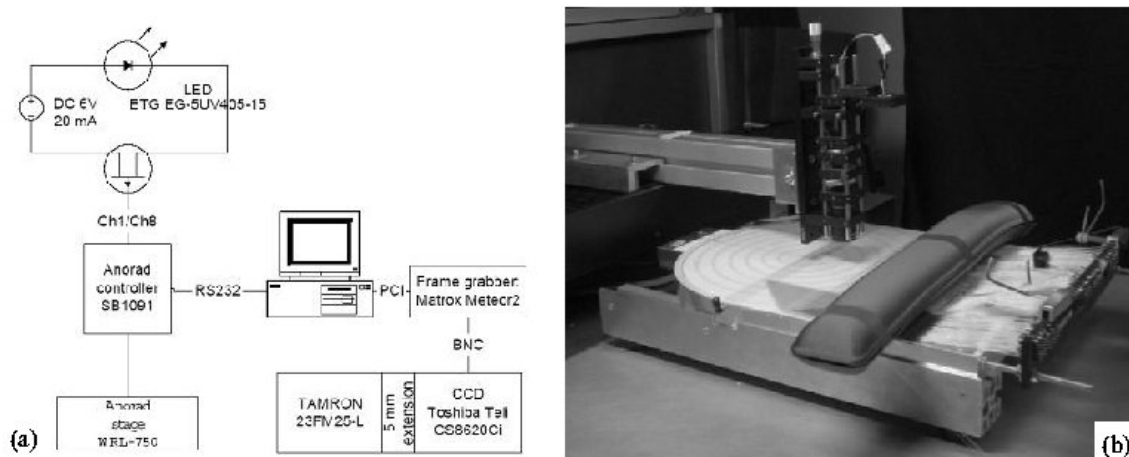
Figure 11: (a) Schematic diagram of the QA system. (b) An overall view of the station assembly QA setup. The optical system is attached to a linear stage and held over the plane of scintillating fibres to illuminate the channels in sequence. The doublet layer is laid on top of a vacuum chuck, which is fixed in place by a guiding rail. The bundled fibre ends are held up in order at the right hand side to be viewed by a CCD camera that is located outside this photograph.

features such as bond wires, the projected line will have soft edges and internal structure when in focus. A mechanical slit was therefore used to select a well-defined, uniformly lit region close to the first focus and the image of this slit was projected onto the doublet layer by the second stage of the optical system which consisted of a matched pair of conventional lenses. This approach also provided a clear working distance between the optical system and the surface of the doublet layer, reducing the risk of damage to the fibres during the scanning process.

Each doublet layer was scanned, after bundling was complete, to ensure that the correct bundles of seven fibres had been grouped together. This was achieved by performing a 'counting-and-ordering check' in which the number of fibres illuminated was counted and the illumination sequence was checked against that expected as the stage passed across the doublet layer. Any errors identified were corrected and the counting-and-ordering check repeated. The fitting of the station connectors only started after the correct bundling had been achieved.

Once all the connectors had been fitted, the doublet layer was scanned at a constant speed of 1.25 mm.s$^{-1}$ with a video capture rate of 25 Hz to allow the fibre-sequence to be verified. For each frame the $3 \times 3$ pixels around the centre of the illuminated fibre were summed. A search was then made through neigbouring frames to find the frame in which the intensity of a particular fibre was largest and the frame number for the intensity peak for each fibre was recorded. Plotting the frame number versus the fibre bundle number revealed misplaced fibres. Figure 13a shows an example of the bundle/frame number correlation for perfect sequencing. Figure 13b illustrates a fibre sequence error.

**Station acceptance procedure**

Each completed station was required to undergo an additional phase of QA testing in order to determine the uniformity of the light yield across its active area. This was achieved by measuring
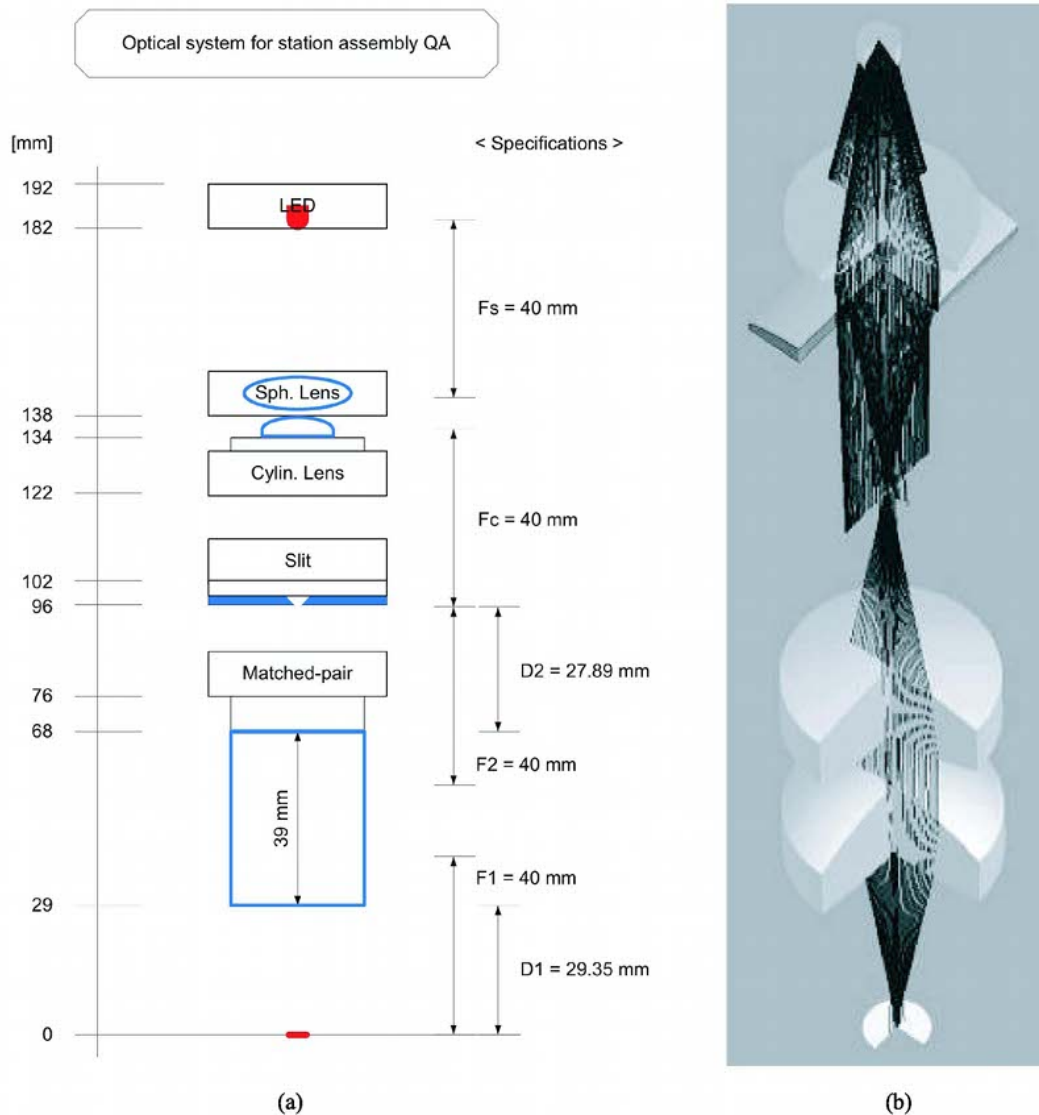
Figure 12: (a) Optical layout of the fibre illuminator. The total optical track is 184 mm from the LED to the image plane. The LED is imaged onto a slit by a combination of a 40 mm focal length spherical lens and a 40 mm focal length cylindrical lens. The slit (50 $\mu$m wide by 4 mm long) is re-imaged onto the fibre by a matched achromatic doublet pair. (b) The diagram shows how the circular beam of light (represented here by ray fans from the LED at the top of the figure) is focused in only one plane by the cylindrical lens to produce a line focus cropped by the slit (tiny shaded bar at the centre), which is then projected on to the doublet layer (at the bottom) by the matched-pair lenses. This diagram was generated from a model of the optical system in the Zemax optical design package [18].
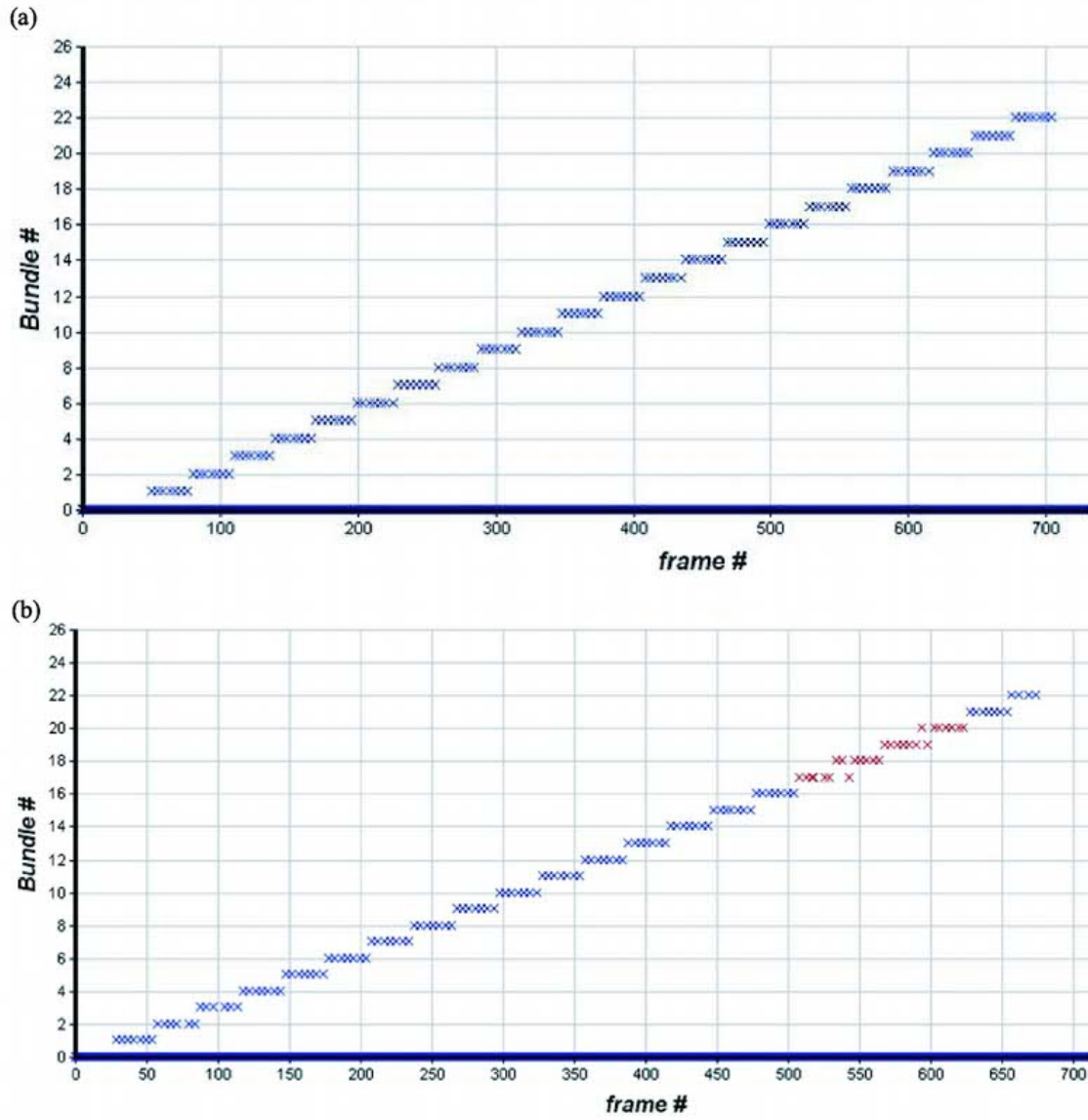
Figure 13: Examples of the plots used to ensure that the fibres were threaded in the correct channel of the station optical connector. The bundle number is plotted against the frame number using the procedure described in the text. (a) Perfect sequencing of all the fibres in the connectors. (b) Single fibres swapped between bundles 17 and 18 and between bundles 19 and 20.
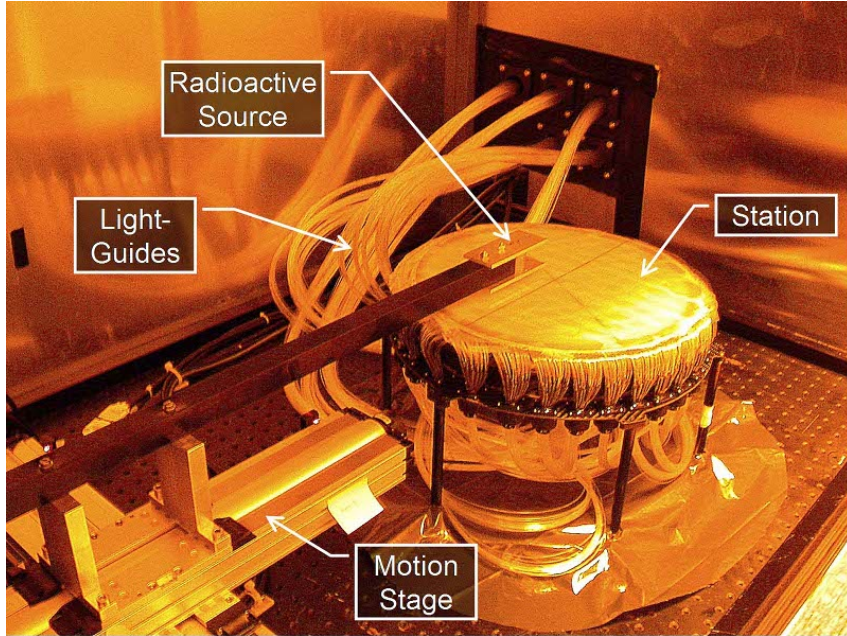
Figure 14: A photograph of a tracker station mounted in the QA test stand. The picture was taken from within the light-tight box which encloses the system. The internal light-guides can be seen connected at the station and the patch panel. The radioactive source was positioned in the holder which was mounted on the motion stage.

the light output by inducing scintillation in localised regions across the surface of the station using a point-like radioactive source. A photograph of the QA test stand in which this process was automated is shown in figure 14.

The station was mounted horizontally on a rigid support frame inside a light-tight box. Scintillation light leaves the box via clear-fibre light-guides and is converted to electrical signals via the 'Visible Light Photon Counter' (VLPC) system described in section 4. Digitisation of the analogue signals from the VLPCs was performed using two prototype 'Analogue Front End' (AFE) boards developed by the DØ collaboration. A collimated radioactive source was held at a fixed distance of approximately 1 mm from the surface of the station. The source could be moved to any location in the plane of the active area by a programmable 2D motion stage, with an absolute position accurate to better than $\pm 5$ $\mu$m.

Initially, a $^{90}$Sr beta source was selected for the QA test stand. It was expected that individual beta particles which passed through all three planes of a station would provide a hit in each of the three doublet layers, providing a clean signature (referred to as a 'triplet') from which the position of the source could be reconstructed. The QA analysis would then compare the reconstructed position with the position set by the 2D stage.

It was found that the overall rate at which data could be read out from the two AFE boards in the DAQ system was limited by hardware synchronisation issues. Due to time constraints and limited availability of equipment, it was necessary to run the AFE boards in 'self triggered' mode rather than with a common external trigger (as will be the case during operation in MICE). In this mode, each board independently determines whether an 'event' should be triggered by
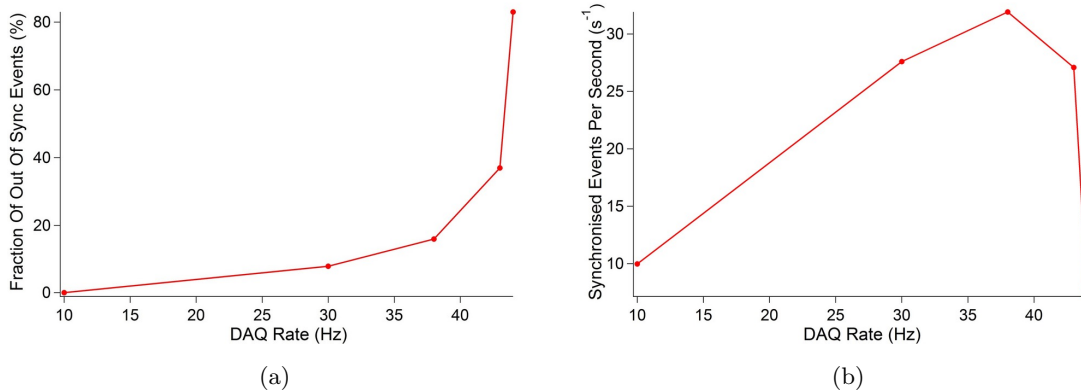
Figure 15: (a) A graph showing, as a function of DAQ trigger rate, the fraction of events acquired from the QA DAQ system in which the data from the two AFE boards are not correctly synchronised. (b) A graph of the synchronised event rate versus DAQ event rate.

comparing the 'OR' of all the signals with a predefined threshold. At high data rates, the AFE boards may each trigger on scintillation light produced by different successive physical stimuli and thus lose synchronisation, leading to invalid data. This phenomenon was investigated by varying the internal AFE thresholds to modify the number of signals accepted as triggers. The fraction of unsynchronised 'events' increased exponentially with DAQ trigger rate, as shown in figure 15(a), limiting the maximum effective readout rate to ∼38 Hz (see figure 15(b)).

In addition to the hardware-imposed rate limits, it was discovered that the mean energy of the $^{90}$Sr beta particles was below that required for penetration through all station planes. Due to absorption and scattering, the number of detected particle hits in each plane decreased with distance from the source such that only ∼4% of recorded events corresponded to a triplet. This resulted in a data rate insufficient for the routine characterisation of tracker stations using only triplet events. It therefore became necessary to consider all events when calculating light yield. The triplet data acquired during the preliminary testing phase were used to calibrate the alignment of the stations with the motion stage coordinate system such that all data values could be mapped to a specific source position using the associated channel number, rather than by reconstructing a complete particle trajectory. Since the triplet rate produced by the beta source was not appropriate for QA purposes, the $^{90}$Sr was replaced by a $^{57}$Co gamma source in the final system. From initial $^{57}$Co measurements it was determined that 50k events were required at each source location to determine the light yield with sufficient precision.

In defining the path that should be traced by the source during a QA test, it was necessary to compromise between the number of channels to be characterised and the overall duration of the scan. Ideally, light yield would be measured with the source placed at a number of points along the length of every fibre channel in each station plane, but the low data rate and large sample size required at each source position rendered this approach impractical. The most efficient scan pattern was therefore defined as the shortest possible path which crosses each channel at least once. The presence of the mirror on one end of the fibre implies that a fault or break in a fibre will reduce the overall light yield regardless of the position at which scintillation occurred.
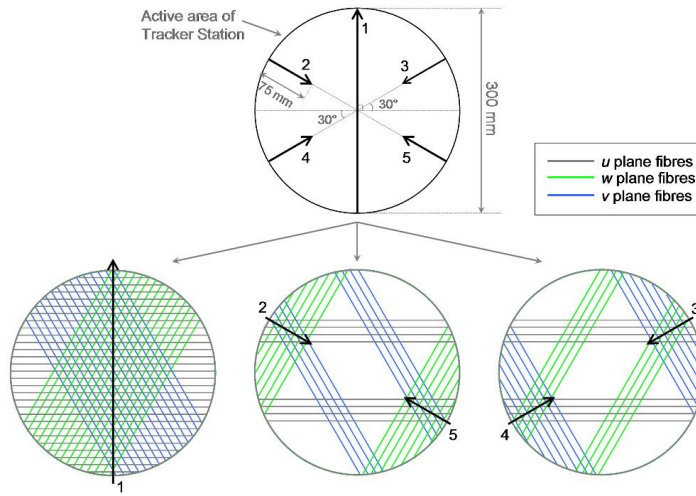
16

Figure 16: A diagram showing the path of the source as it is scanned across the active area of a tracker station during the QA test procedure. Scan 1 is perpendicular to the fibres in plane $u$, and extends across the entire active region. Scans 2 and 5 are perpendicular to the fibres in plane $w$, while scans 3 and 4 are perpendicular to those in plane $v$; each of these scans has a nominal length of one quarter of the active area diameter. The lower portion of the figure illustrates the manner in which subsets of the $u$, $v$ and $w$ plane fibres were illuminated by the source during each scan (not drawn to scale).

Hence, one measurement per channel was judged to be sufficient to identify abnormal fibres for which further investigation was required. The format of the QA scan pattern is shown in figure 16.

Despite simplifying the scan path, the limited time available for the completion of the initial phase of QA testing prior to the assembly of the first tracker was such that only a subset of the channels of each station could be routinely evaluated. It was ultimately necessary to test each station within a period of one day, nominally corresponding to two consecutive 8-hour shifts by the test operatives. Excluding the time required to prepare and install a station in the QA stand (and to remove it following a test run) $\sim$11 hours were allocated for data acquisition. With a requirement of 50k events per source position and a maximum data rate of $\sim$38 Hz, this enabled measurements to be taken at 28 discrete locations during the scan, at intervals of 27.4 mm ($\sim$18 channels). However, had any evidence of light yield non-uniformity been detected at this stage, higher resolution studies of individual channels in the affected area would have been made. No evidence of such a non-uniformity was observed.

## 2.2 Light-guides and optical connectors

### 2.2.1 Light-guides

Clear-fibre light-guides are required to transport light from the scintillating-fibre stations to the VLPC readout system. Kuraray clear polystyrene, round, s-type, 1.05 mm fibre was chosen for the light-guides [19]. The attenuation length of the fibre was measured to be 7.6 m and thus,

17

Table 2: Light-guide lengths. The serial number is a tracking number marked on the connectors. Tracker 1 is for the upstream spectrometer and tracker 2 for the downstream spectrometer. Station 5 is located nearest to the patch panel, and station 1 is furthest from the patch panel.

| Serial Number | Tracker | Station | Internal | External |
|---|---|---|---|---|
| 6-10 | 1 | 5 | 1500 mm | 2500 mm |
| 16-20 | 1 | 4 | 1950 mm | 2050 mm |
| 21-25 | 1 | 3 | 2250 mm | 1750 mm |
| 26-30 | 1 | 1 | 2600 mm | 1400 mm |
| 31-35 | 1 | 2 | 2400 mm | 1600 mm |
| 36-40 | 2 | 5 | 1500 mm | 2500 mm |
| 41-45 | 2 | 4 | 1950 mm | 2050 mm |
| 46-50 | 2 | 3 | 2250 mm | 1750 mm |
| 51-55 | 2 | 2 | 2400 mm | 1600 mm |
| 56-60 | 2 | 1 | 2600 mm | 1400 mm |

to reduce the light loss in propagation as far as possible, the length of the clear-fibre run from station to VLPC cassette was specified to be 4 m.

The light-guide, a bundle of 128 clear fibres, is composed of an internal section, which connects between the station and the patch panel, and an external section, which connects between the patch panel and the VLPC cassette. The external light-guide is equipped with a flexible tube which shields the fibres from ambient light and also protects the fibres from any damage during handling and assembly. The length of each light-guide is summarised in table 2. Optical grease was applied to all optical connectors when mating the light-guides in order to minimise light yield loss due to Fresnel reflection.

Each internal light-guide (figure 17 top) has one 128-fibre 'patch-panel' connector (1A) and six 22-fibre station connectors (3A). The connector 1A (figure 18 top-left) has 128 holes which match with those of the connector 2A (figure 18 bottom-right) of the external light-guide. The connector 3A (figure 18 top-right) has 22 holes configured as shown. These connect to the station connector and are locked by the collar 3B.

The external light-guides (figure 17 bottom) use a 128-fibre optical connector, developed by DØ, at the end that interfaces to the VLPC cassette and a connector assembly (2A-E) which mates to connector 1A of the internal light-guide. Flexible tubes F1, F2, and F3, and heat-shrink tubes S1, S2, S3, and S4 form the body casing of the external light-guide. A light-tight injection-moulded boot (2F) is glued into the rear of the DØ connector and flexible tube F1 is attached to the boot using sleeve 2G with adhesive and heat-shrink tubing S1. This makes the assembly fully light tight and adds strength. The flexible tubes F1, F2, and F3 are fixed with heat-shrink tubes S2 and S3. The locking ring 2B is used for securing the connector 2A to the connector 1A of internal light-guide at the patch panel. The optical connector DØ (figure 18 bottom-left) has 128 holes, in a $16 \times 8$ arrangement which make contact with the connector
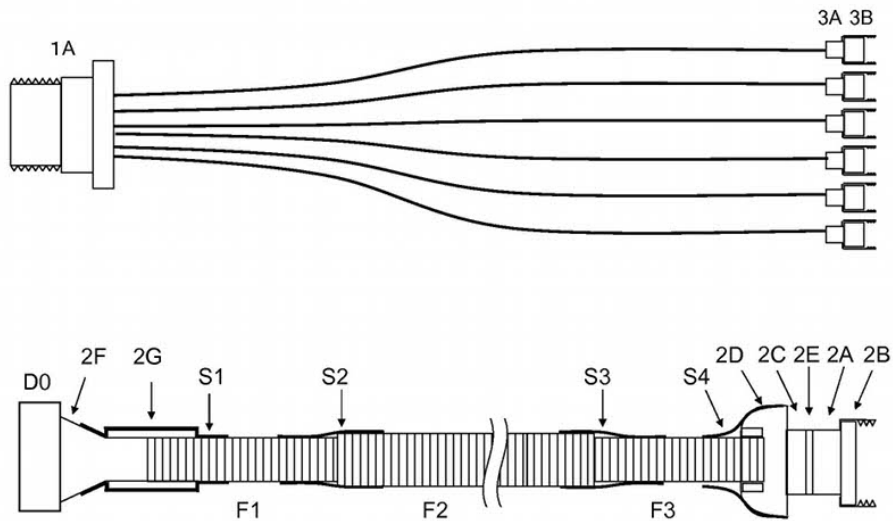
Figure 17: Drawings for internal light-guide (top), and external light-guide (bottom). 1A, 3A, DØ, 2A are optical connectors; 3B, 2B are locking rings.
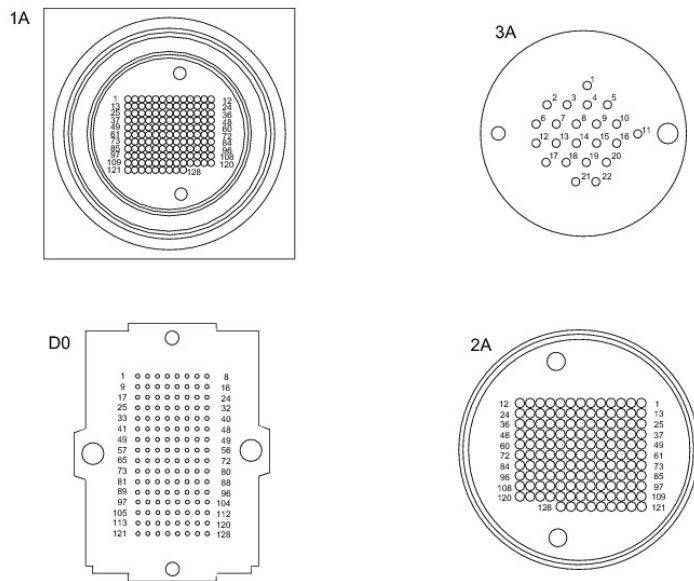


Figure 18: Schematic view of optical connectors. The connector 1A (top-left) and 3A (top-right) are for the internal light-guide, DØ (bottom-left) and 2A (bottom-right) for the external light-guide.

at the VLPC cassette. The optical connector 2A (figure 18 bottom-right) has 128 holes in an arrangement as shown, which mates with connector 1A of the internal light-guide.

### 2.2.2 Light-guide fabrication

Five-metre lengths of fibre were cut from the spool on which they were delivered by the man-ufacturer. A bundle of fibres was then connected to cookies at each end in order to perform the first transmittance measurement (see below). Fibres passing the transmittance test were cut into two pieces, one for the internal light-guide and the other for the external one. Next, optical connectors were attached at each end of the bundle and glued in position to allow the first polishing step to be performed. A second transmittance measurement was then performed. The connectors that passed this test were polished using a diamond cutter.

### 2.2.3 Light-guide quality assurance

After a brief inspection of the fibre connections, three quality assurance steps were carried out. The first step was to search for evidence of kinks or cracks in the fibres produced in handling the light-guides during manufacture. The surface of each connector was exposed to a strobe light and the reflected light was captured in a photograph taken with a digital camera. An example of such a photograph, showing evidence of damage in one fibre, is shown in figure 19. The damaged channel is clearly visible in the photograph where the injected light is reflected from the damage point along the fibre. The second QA step was to measure transmittance in the fibres. The bundle of fibres was illuminated using a diffuse source of green light (see figure 20). The light transmitted along the light-guide was observed with a CCD camera. The variation in light transmission from fibre to fibre was found to be less than 10%. The fraction of fibres with transmission less than 90% (of the average) was less than 0.7%. Finally, the fibre mapping at each connector was checked.

### 2.2.4 Optical connectors

The station optical connector is shown in figure 21 together with the various gauges used in the station-connector QA. The connector has 22 1.05 mm-diameter holes, drilled to take the fibres, and was machined from black Delrin. The alignment dowels have different diameters, 2 mm and 2.5 mm, to prevent any possibility of mating the connector pair in the wrong orientation. To ensure that the two halves of the connectors have no misalignment (which would cause light loss) a set of gauges was manufactured. These consisted of a plate in which a series of dowels were accurately positioned at the locations where the holes in the connector should be. A separate gauge was made for each half of the connector. To check the accuracy of the two gauges, a precisely drilled plate was produced. All of the connectors were checked using one of these gauges, and any that failed were discarded.

Figure 22 shows the patch-panel connector components. The connector bearing the square flange is fitted to the internal light-guide and incorporates an O-ring to make a gas seal. The patch-panel connector is machined from black Delrin. There are six station connectors to each patch-panel connector, though not all of the channels in all the station connectors are used.
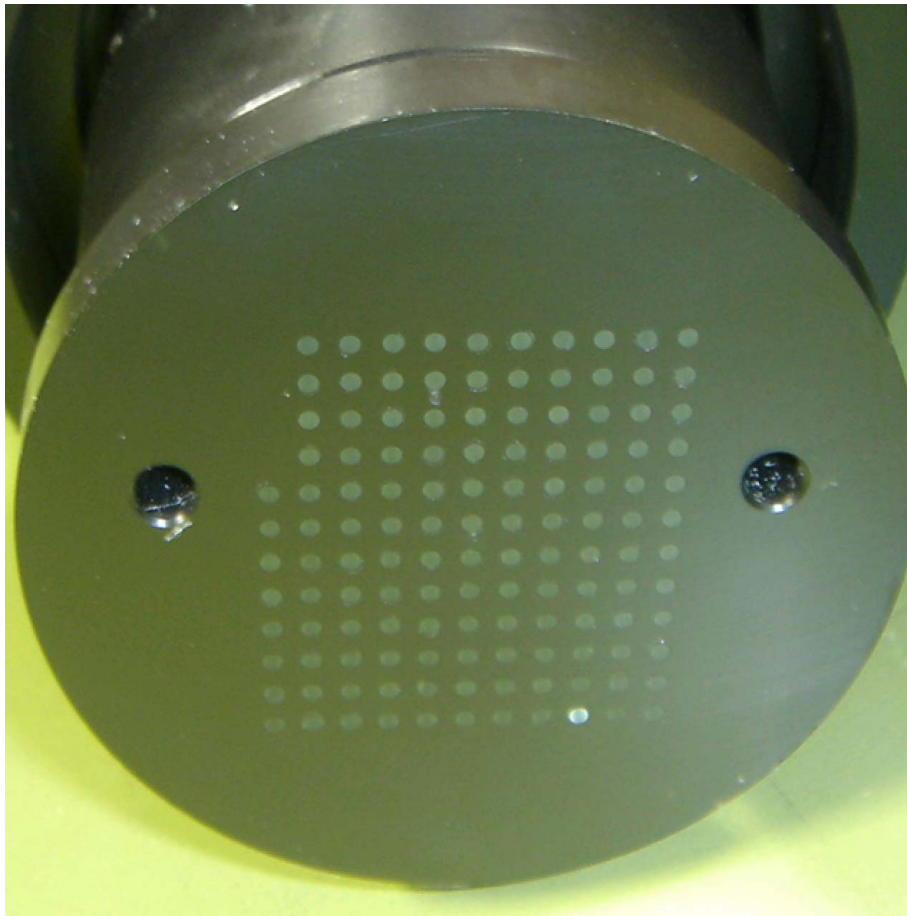
Figure 19:  Photograph of the connector surface taken with strobe illumination. Reflected light is seen in a fibre at the bottom.
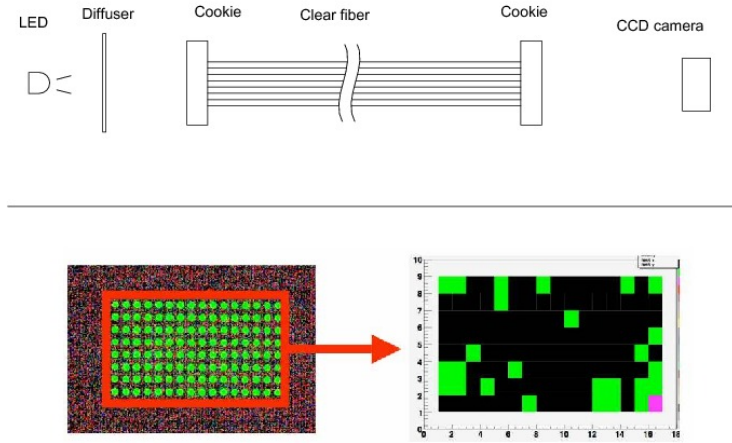
Figure 20: Setup for transmittance measurement (top). The light from the green LED passes through a diffuser and illuminates the fibres. The intensity of the transmitted light is measured using a CCD camera. The CCD image of transmitted light (bottom-left) is analysed and the intensity of the green component in each fibre is checked. The intensity of each channel, relative to the average for the light-guide under test, is plotted channel by channel (bottom right). The red pixel indicates a channel with a transmitted light intensity 8% lower than the average.



Figure 21: The station connector gauge set. The gauges are arranged in a row at the top of the photograph. The left- and right-hand gauges were used to check the connector part shown directly below. The 'gauge gauge' shown in the centre of the top row is used to ensure that the pins in the two gauges are precisely matched.

Figure 22: Components of the patch-panel connector. (a) The components before assembly. The bulkhead connector carries a square flange to carry an O-ring and to allow the connector to be held with screws onto the patch panel. The mating connector with locking ring is shown as well as the strain relieving piece (the lightly shaded ring) that is attached to the external light-guide. (b) The assembled patch-panel connector.
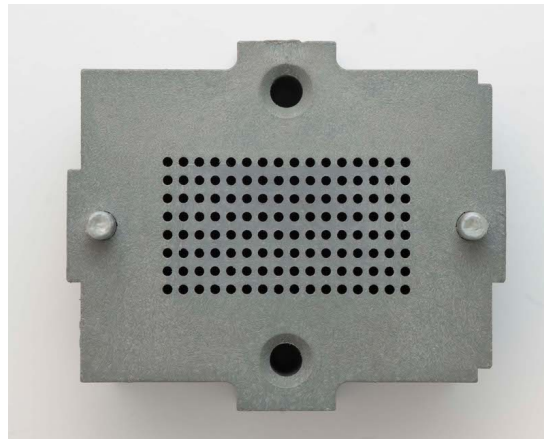


Figure 23: DØ warm-end optical connector.

The optical signals are fed from the patch-panel to the VLPC system via the external light-guides, each containing 128 fibres. The light-guides terminate in the DØ warm-end connector shown in figure 23. This is an injection-moulded part, also made from Delrin. The figure shows the 128 holes for fibres, two holes (left/right) for alignment pins and two holes (top/bottom) for threaded inserts. Light-guide fibres of 1.05 mm diameter are used while the DØ VLPC cassettes use fibres of 0.965 mm diameter. This mismatch results in a light loss of ∼15%.

## 2.3   Tracker assembly and integration

### 2.3.1   Assembly

The stations to be used in the final trackers were chosen on the basis of the results obtained in the QA exposure of the stations to the radioactive source. The stations that make up a tracker
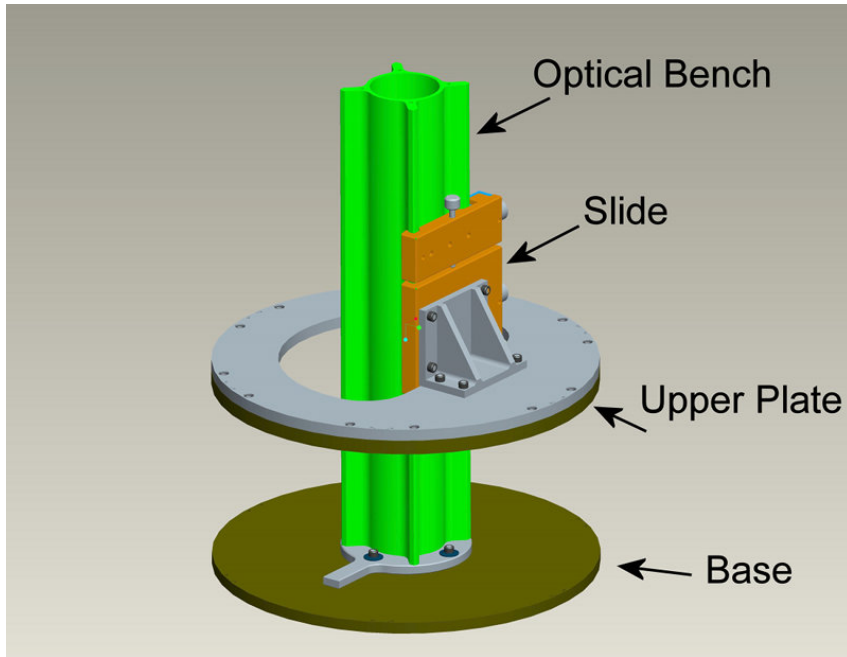
Figure 24: Engineering model of the gluing jig showing the base plate (labelled 'base'), the optical bench and slide, and the upper plate. The space frame was held in position between the upper plate and the base plate while the glue was allowed to cure.

are held in position using four carbon-fibre space frames. The relative positions of the stations were determined using the following assembly procedure.

Each space frame was assembled in a gluing jig (see figure 24) which consisted of an optical bench fixed to a base that included dowel holes matching those in the station bodies. A similar plate was mounted on an optical slide and the distance between this plate and the base plate could be adjusted and set precisely. The distance between the two plates was checked, not only to ensure the correct inter-station distance, but also to ensure that the two plates were parallel.

The four sections of the carbon-fibre space frame consist of 25 components: 12 feet; 6 inter-station tubes; 6 'W' sections; and a stiffening tube. Each section was assembled between the two plates of the gluing jig (figure 24) and bonded. When the assembly had fully cured it was removed from the jig and measured; the jig was then reset to the next inter-station pitch.

It was a simple matter to assemble the stations and space frames into a complete tracker as all the joints are doweled. When a complete assembly was finished it was measured using a CMM to verify the position of each station relative to the axis of the tracker. The axis of the tracker was taken to be the line joining the centre of the active area of station 1 with the centre of the active area of station 5. The centres of stations 2, 3 and 4 were then determined and reported as deviations from this axis. The distance between the stations was determined by taking the mean of four position measurements taken from the machined face of the station flange. Figure 25 shows the position of each station in the first MICE tracker. The precise measurements of the station positions have been used in the reconstruction of the data from the first MICE tracker
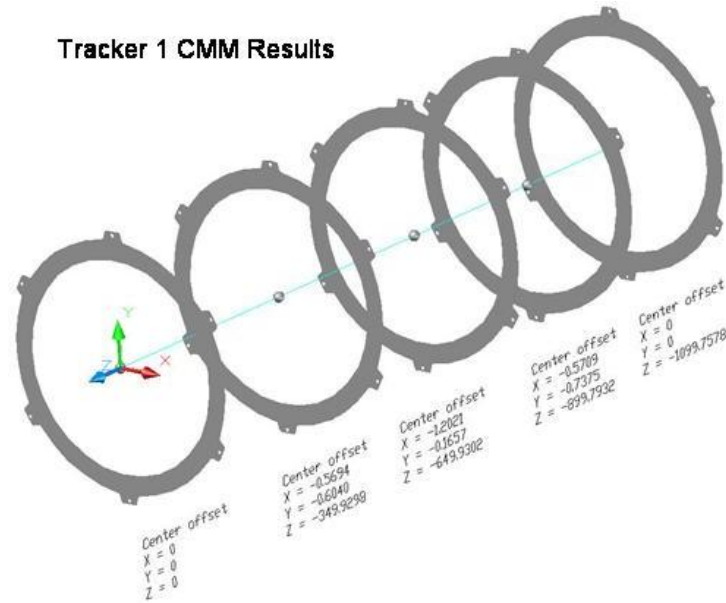
Figure 25: Representation of the measured positions (in mm) of the five stations of the first MICE tracker. The centres of stations 2, 3, and 4 were determined relative to the centres of stations 1 and 5 and the $z$ position of stations 2, 3, 4, and 5 were determed relative to the position of station 1 as described in the text.

that is presented below.

### 2.3.2 Integration

The installation of the tracker into the spectrometer solenoid bore will have to be carried out in UV-filtered light to avoid any degradation of the scintillating fibres. To achieve this, a blackout tent will be erected around the end of the solenoid and made light tight. Specially filtered lighting will then be installed in the tent allowing the tracker to be removed from its light-tight container and placed on the installation platform. The platform is adjustable to enable the tracker to be aligned with the bore of the solenoid. When on the platform, the frame that will support the internal light-guides during the installation will be attached to the tracker via a flexible coupling to ensure that no stresses are transferred to the tracker during the fitting of the internal light-guides (see figure 26). The light-guide connections will be checked to ensure that the light-guides are correctly positioned and labelled.

With the internal light-guides attached, the tracker assembly (consisting of the tracker, the light-guide support, and the light-guides) is ready for installation. If necessary, the tracker assembly can be stored in an extended light-tight storage tube for installation at a later date. For installation, the complete tracker assembly is slid into the solenoid bore to the correct '$z$' position. The tracker will sit on four adjustable feet, two at each end. The adjustable feet will be used to align the tracker with the magnetic axis of the solenoid. Once this has been done, the location bracket will be fitted. The location bracket locks the tracker in its $z$ and azimuthal positions (see figure 27).
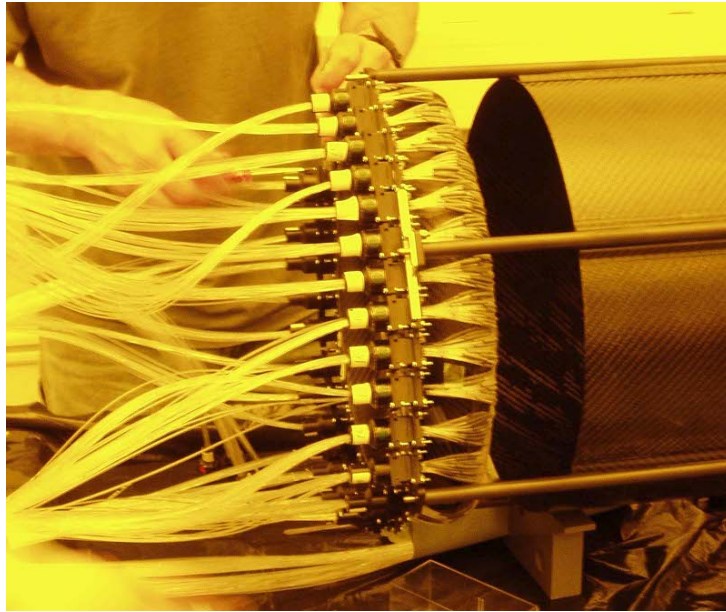
Figure 26: Photograph of assembled tracker showing the internal light guides being attached to the support frame by which they are supported during the installation of the tracker into the bore of the solenoid. In the picture, the tracker is being prepared for installation in the light-tight carbon-fibre tube used to house the tracker in the cosmic ray test stand.
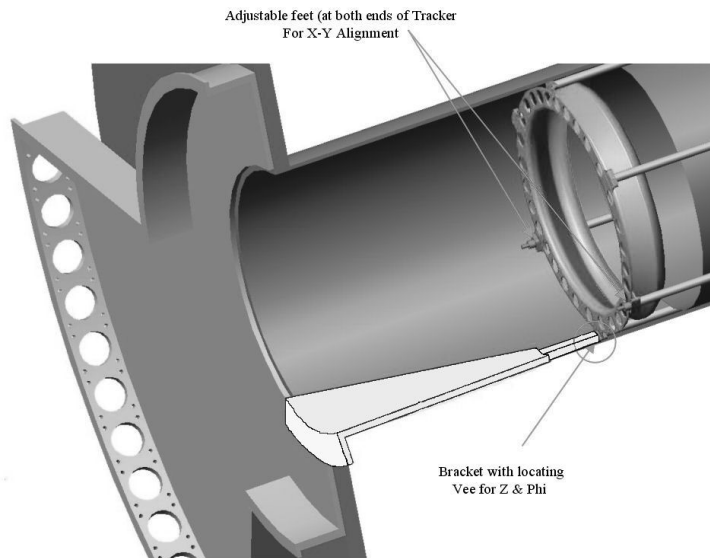


Figure 27: Tracker alignment mechanism. The lighter part shown will be dowelled to the spectrometer solenoid end plate. At the narrow end of the part, inside the bore of the solenoid, a locking mechanism will be used to locate the tracker in $z$ and in azimuth.
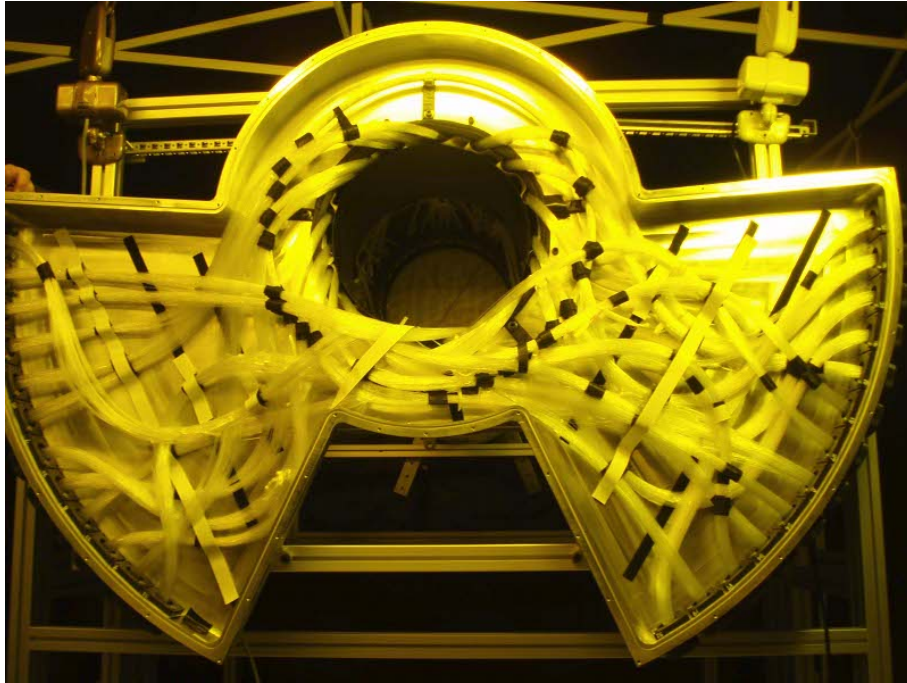
Figure 28: Photograph of the internal light-guides supported within the patch panel. The photograph was taken at the end of the assembly of the first tracker in the cosmic test stand. The light-guides are held out of the tracking volume using a sprung carbon-fibre collar inserted into the the bore.

The light-guides will now be removed one-by-one from the support frame and fitted into the patch panel. This is a procedure that requires great care to ensure that the fibres are not damaged and a collar will be fitted to ensure that the bore is kept clear (see figure 28). Finally, the patch-panel cover will be fitted and, if the external light-guides are to be fitted at a later stage, the patch panel connectors will have their light-tight caps fitted.

# 3 Photon Detection System

The photo-detection system for the MICE trackers is built on the success of the system built for the DØ experiment [12]. The DØ Central Fiber Tracker (CFT) is read out using Visible Light Photon Counters (VLPCs) [13, 14]. The extremely high quantum efficiency of the VLPCs was essential for the performance requirements of the DØ experiment to be met and, for MICE, has allowed a very aggressive fibre-tracker design based on 350 $\mu$m diameter fibres to be developed. The MICE trackers will use DØ CFT readout and front-end electronics (on loan from the DØ experiment).

## 3.1 Visible Light Photon Counter - VLPC

The light produced from charged particles passing through the scintillating fibres is piped along the fibres and thence, via the clear-fibre light-guides, to the VLPCs, which are housed in cassettes
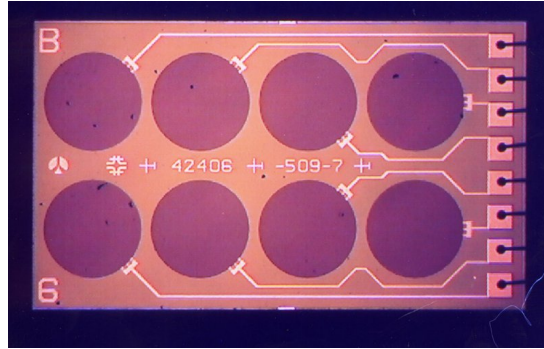
Figure 29: Photograph of the 8-element VLPC array.

(see below) and which convert the light into an electrical signal. The VLPC is a silicon-avalanche device operated at cryogenic temperature. It is a development of the Solid State Photomultiplier, an impurity-band silicon avalanche photo-detector. It has undergone six design iterations, specified as HISTE I to HISTE VI. HISTE VI, the version used in the DØ CFT, and thus the version that is used in MICE, is an eight element array in a 2-by-4 geometry, (figure 29) with each pixel in the array having a diameter of 1 mm. The HISTE VI operational parameters are: quantum yield, $> 0.75$; gain $(G)$, 20,000–60,000; operating temperature, 9 K; and operating bias, 6–8 V.

VLPCs are fabricated using an epitaxial growth process which produces a series of doped and undoped silicon layers on highly-doped silicon substrate wafers. Each eight-pixel chip (figure 29) is soldered to an aluminium nitride substrate. The outputs from individual pixels are wire-bonded to individual contact pads on the substrate. VLPCs from different batches exhibited a large variation in gain due to non-uniformities in the production process [20]. Due to these variations, the VLPCs were selected from individual wafers and sorted into like-gain batches with small gain dispersion. MICE will be using cassettes with gains of approximately 40k and approximately 20k.

## 3.2   VLPC cassettes and cryostats

The VLPC cassette contains 1024 channels of VLPC readout and is divided into 8 modules of 128 channels each. The modules are interchangeable and may be removed for repair. This is illustrated in figures 30 and 31. Figure 30 shows the full cassette with readout boards attached. Figure 31 shows the inner components of the cassette, with the readout boards and cassette body removed. Sitting directly over each VLPC pixel is an optical fibre which brings the light from the detector to the VLPC chip. Each cassette module is composed of an optical bundle assembly, a cold-end electronics assembly, and an assembly of mounted VLPC hybrids. The high-cost and delicate nature of the cold-end assembly led to the development of a design that allows the cold-end assembly to be removed easily for repair. Another important design requirement for the cassette regards the readout electronics. Due to the nature of Tevatron operations, it must be possible to remove and replace the readout electronics boards, the front-end boards which act

as the interface to the data acquisition system, without removing a cassette from the cryostat. The readout electronics are discussed in detail in section 4.

The cassette has a 'cold end', that portion of the cassette which lies within the cryostat, and a 'warm end', the portion of the cassette which emerges from the cryostat and is at room temperature. At the cold end, eight 'cold-end assemblies', each of 128 channels of VLPC readout, are hung from the feed-through by the optical bundles and are surrounded by a copper cup. Each cold-end assembly consists of sixteen, 8-channel VLPC hybrid assemblies, the 'isotherm' or base upon which they sit, the heater resistors, a temperature measurement resistor, cold-end flex-circuit connectors and the required springs, fasteners and hardware (see inset in figure 30). Running within the cassette body from top to bottom are eight 128-channel optical-bundle assemblies which accept light from the detector light-guides connected to the warm-end optical connectors at the top of the cassette and pipe the light to the VLPCs mounted at the cold end (see figure 31). The electronic read-out boards are located in rails which are mounted on the warm end structure and are connected electrically with the cold-end assemblies via kapton 'flex circuits'. In addition, the electronics boards are connected to a backplane card and a backplane support structure via multi-pin connectors and board-mount rails. The flex circuits and read-out boards are electrically and mechanically connected by a high density connector assembly. For more details on the VLPC cassette design see [12].

Since the VLPCs operate at cryogenic temperatures, a helium cryo-system is required. A special purpose cryostat has been designed and built for MICE to allow the VLPCs to be operated at a temperature of $(9.0 \pm 0.1)$ K. The cryostat has two cassette slots which accept DØ 1024 channel VLPC cassettes (see figure 32). The MICE VLPC cryo-systems use Gifford-McMahon cryocoolers (Sumitomo RDK 415D [21]) to maintain the 9 K operating temperature for the VLPCs. This two-stage, commercial cryocooler is located between the two cassette slots. The first stage of the cryocooler, operating at 50 K, is used to provide a heat intercept between the room-temperature cryostat body and the cold-end assembly. The cold head of the cryocooler is used to cool the copper isotherm in order to bring the VLPCs to their operating temperature. The 50 Hz mains frequency employed in the UK results in the cryocooler operating at about 70% of its rated capacity. The cryocooler, along with its helium compressor, gas flex lines, and control cables is provided by the manufacturer as a packaged system. The system has worked flawlessly, providing a stable, non-fluctuating temperature at the cold-end assembly for long operating periods.

The cassette envelope is a low conductivity, low thermal-expansion box that seals to the underside of the top lid of the cryostat. The insulating vacuum is on the outside of the envelope and the VLPC cassette, immersed in helium gas, is situated inside the envelope. The nominal clearance inside the cassette is made rather tight at 0.6 mm in order to facilitate heat conduction to the cryocooler. The wall thickness, 0.38 mm, was also reduced to the minimum practical for fabrication so as to minimise heat conduction along the cassette envelope from the warm end to the cold end.

Thermal links provide the conduction heat-transfer path between the two stages of the cryocooler and the cassette. The thermal links are made from oxygen-free high-purity copper
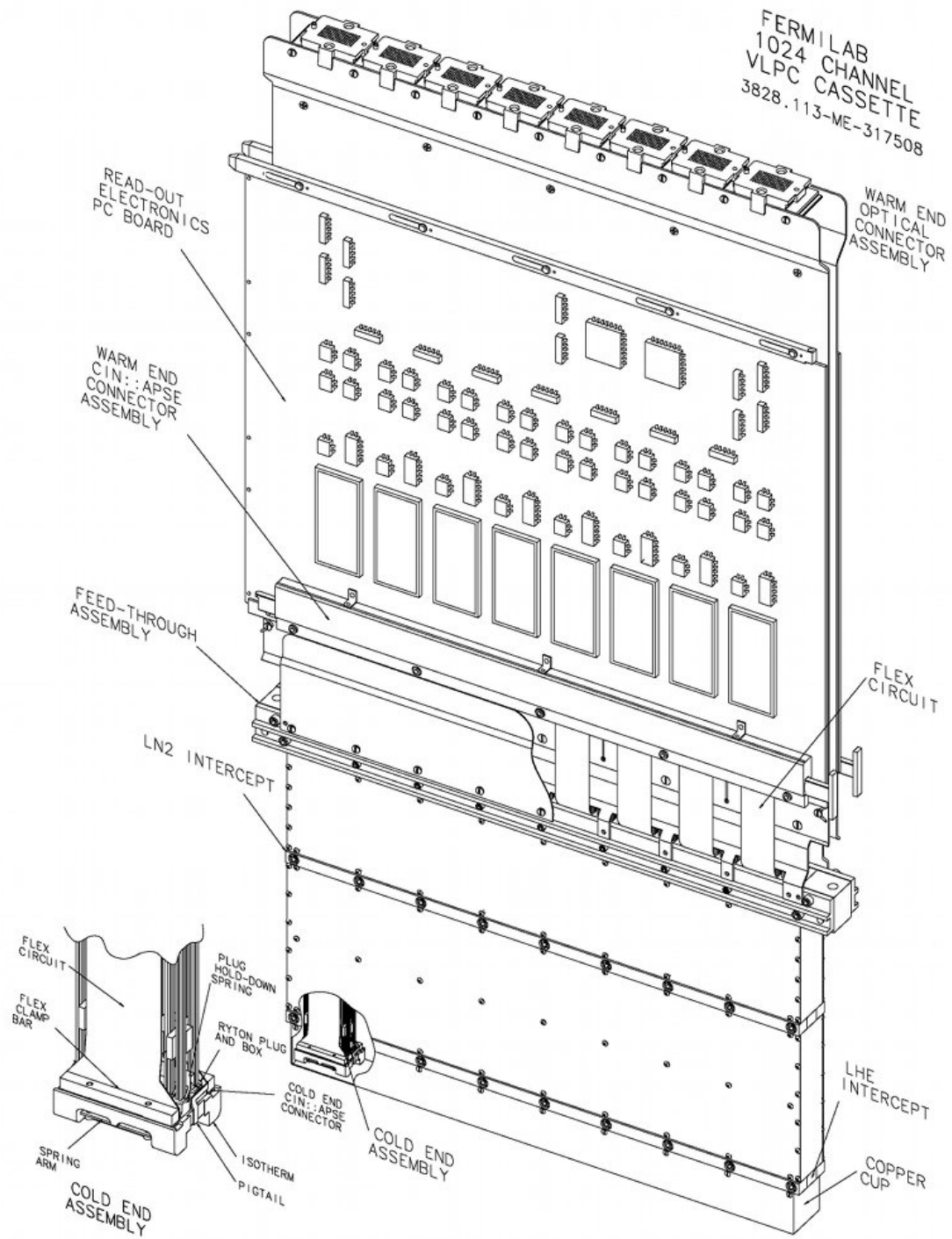
Figure 30: A VLPC cassette supporting AFE readout boards as viewed from the left side. The VLPC hybrids are located on the isotherms housed inside the copper cup shown at the bottom of the figure. This figure was published in Nuclear Instruments and Methods A, A565, V.M. Abazov et al., pg. 463-537, Copyright Elsevier (2006).
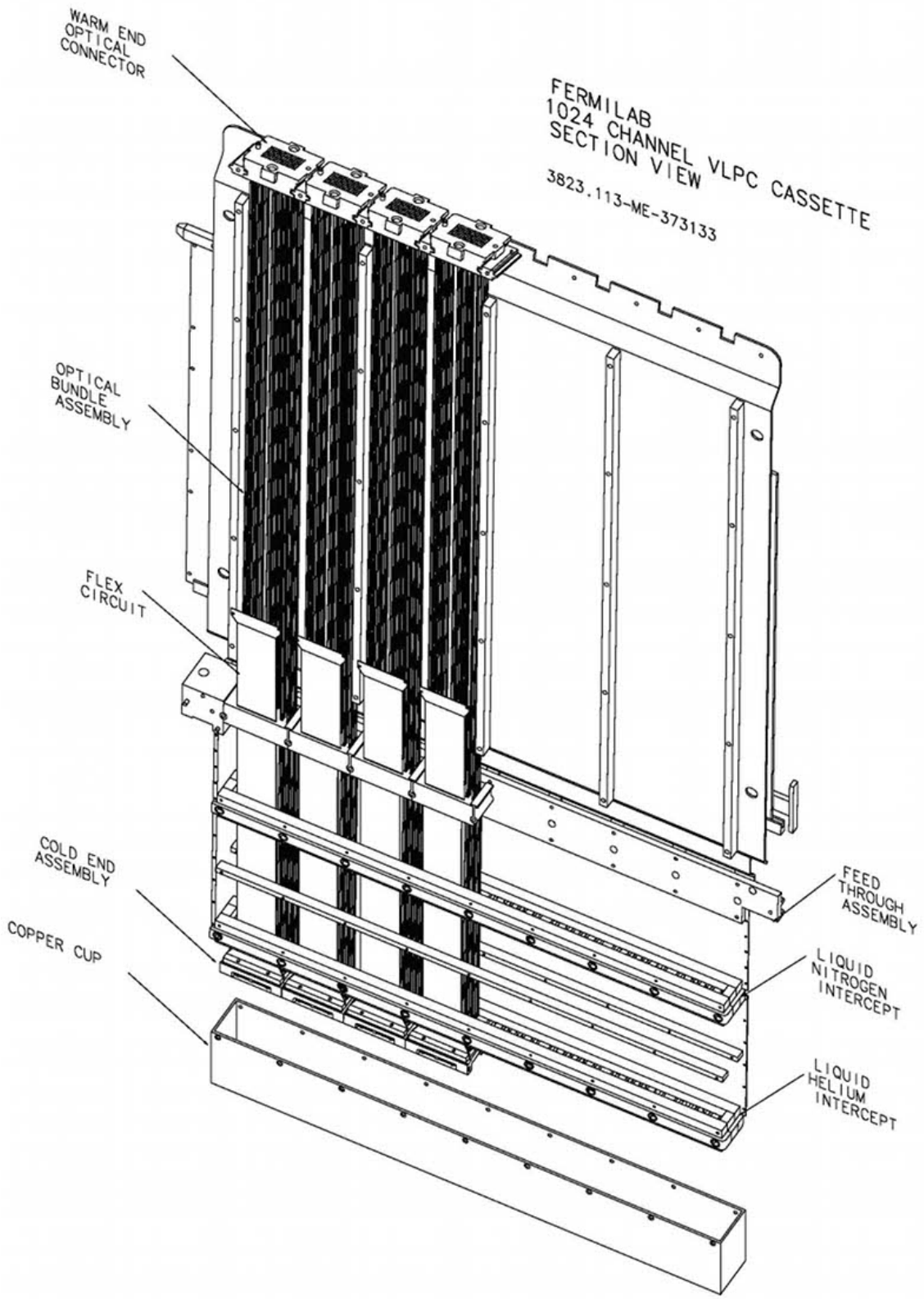
30

WARM END
OPTICAL
CONNECTOR

FERMILAB
1024 CHANNEL VLPC CASSETTE
SECTION VIEW
3823.113-ME-373133

OPTICAL
BUNDLE
ASSEMBLY

FLEX
CIRCUIT

COLD END
ASSEMBLY

COPPER CUP

FEED
THROUGH
ASSEMBLY

LIQUID
NITROGEN
INTERCEPT

LIQUID
HELIUM
INTERCEPT

Figure 31:   VLPC cassette body with left side body panel and side panels removed to show four installed modules.  This figure was published in Nuclear Instruments and Methods A, A565, V.M. Abazov et al., pg. 463-537, Copyright Elsevier (2006).

31
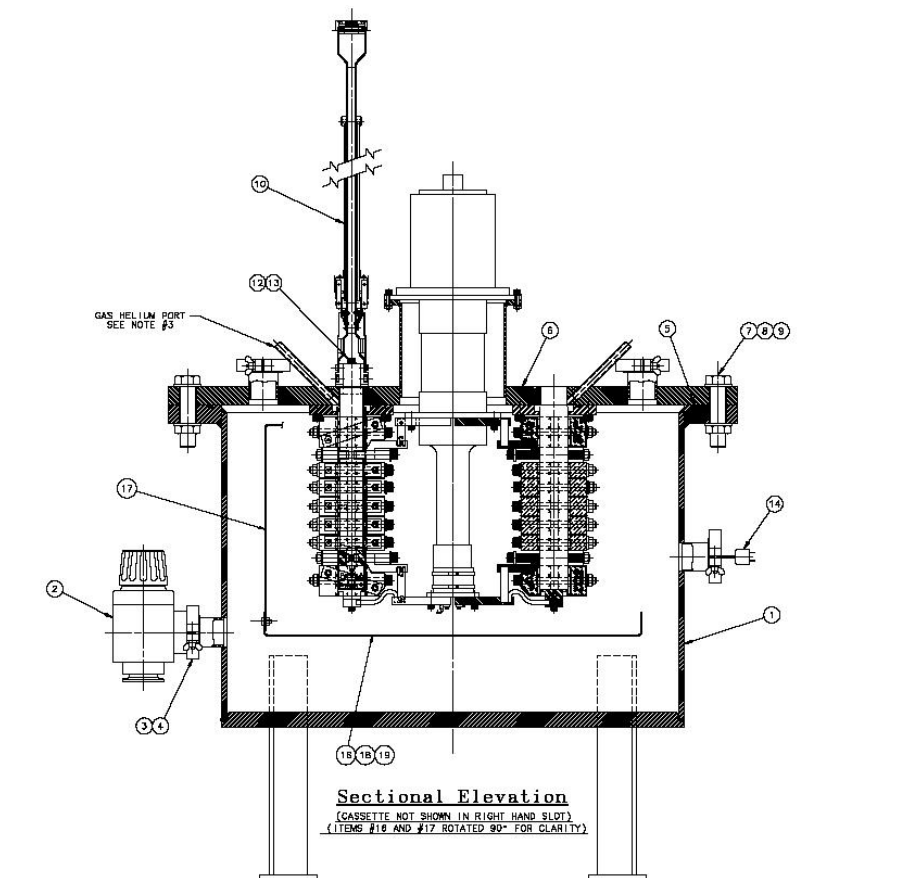
Figure 32: Sectional elevation drawing for the MICE 2-cassette VLPC cryostat.

Figure 33: Close up of the lower thermal link flexible section. The cassette envelope may be seen on the left-hand side of the picture. The copper foils that form the thermal link between the cold end and the cryocooler cold head may also be seen. The Cernox temperature sensor is mounted to the envelope side of the link.

(OFHC), UNS grade C10100. The thermal links are 10 mm thick solid copper pieces with a short flexible segment to accommodate a movement of 2 mm due to thermal contraction. The flexible segment is constructed of 35 individual 0.13 mm thick pieces of high purity copper foil soldered to the solid segments. The upper thermal link operates at a temperature of around 45–50 K and has a temperature gradient of 1 K from the cryocooler connection to the envelope connection. The lower thermal link (figure 33) operates at temperatures in the range of 6–8 K and has a calculated 0.1 K temperature drop from the cryocooler to the envelope.

Cernox temperature sensors from Lakeshore Cryogenics [22] are mounted on the cold head of the cryocooler and the lower thermal link near the cassette envelope. A silicon diode temperature sensor from Oxford Instruments is used to measure the upper link temperature. A 100 Ω platinum resistor was also used during the commissioning tests. The sensors are mounted into small copper holders using GE-7031 varnish. The copper holders themselves are screwed to the surfaces with a #4-40 screw with Apiezon 'N' grease at the interface. Cryogenic quad-lead wire from the sensors is heat-sunk to a small copper bobbin mounted nearby. Readout and temperature control is via an Oxford Instruments, ITC503 temperature controller. A flexible 36 Ω heater element is wrapped around the second stage of the cryocooler using high purity copper sheeting and hose clamps. The heat transfer surface of the heater is lightly coated with Apiezon grease. Up to 5 W of heat can be supplied by the heater to give gross temperature control for the cassette cold end. Each cassette also has individual heater controls (one heater for each module in a cassette for a total of 8) to adjust for small, asymmetric temperature differences.
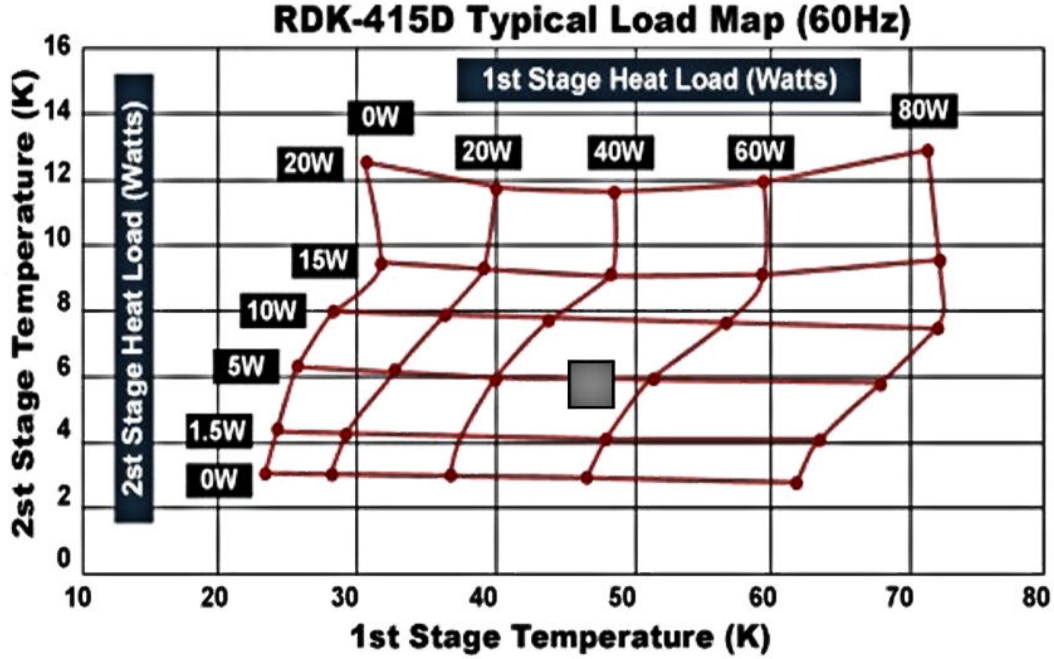
Figure 34: Load map of the Sumitomo RDK 415D cryocooler. The square indicates the system operating envelope with no additional heat (via stage II heater). Figure taken from [21].

Although we experienced some difficulty in making good (high-conductance) connections on the thermal links at the cryocooler head and the cassette envelope, once good link connections had been made, the system performed extremely well. Figure 34 shows the load map for the RDK 415D. This agrees well with the operating point expected from heat load calculations based on the cryostat and VLPC cassette engineering designs. In normal operating conditions, a small amount of heat is added to stage II using the heater (supplied and controlled by the Oxford controller) giving better temperature stability. With full control (Oxford and cassette temperature control on), the VLPC temperature is controlled at $(9 \pm 0.005)$ K.

# 4    Electronics and data acquisition

MICE uses the DØ Central Fiber Tracker (CFT) optical readout and electronics system. Two Analogue Front End (AFE) boards are mounted on each VLPC cassette. The AFE boards read out 512 channels each and provide VLPC bias and temperature control functions.

## 4.1    AFEIIt Boards

The board used in MICE is the second generation front-end readout board, the AFE-IIt [15]. As shown in figure 35, the analogue pulses produced by the VLPCs are input to 'Trigger and Pipeline with timing' (TriP-t) chips on the AFE-IIt boards. The TriP-t chip generates three outputs for each channel: a digital discriminator signal; an analogue pulse proportional to the

amplitude of the integrated charge of the input pulse (the A-pulse); and an analogue pulse (the t-pulse) proportional to the time between the firing of the discriminator and the closing of the time gate.

The discriminator output is routed to one of the Field Programmable Gate Arrays (FPGAs), the DFPGA (Digital or Discriminator FPGA). The A-pulse and the t-pulse are stored in 48-sample, analogue pipelines in the TriP-t chip before being read out upon the receipt of an external Level 1 accept (L1ACCEPT) trigger. In MICE the discriminator bits, which indicate which channels are above a predetermined threshold, will be directed to another FPGA called the AFPGA (Analogue FPGA), and will be used to suppress the digitization cycle for channels that are below threshold. MICE will use a scheme in which only those channels above threshold are digitised. This scheme will decrease the digitization time for an event. The high L1ACCEPT rate (600 kHz) anticipated in MICE has required this implementation of the Digitise-Readout mode structure.

In DØ, a TriP-t chip receiving a L1ACCEPT signal causes the AFE-IIt board to direct the TriP-t chip to execute 'Acquire', 'Digitise', and 'Readout' cycles for the A-pulse and t-pulse from a fixed location in the pipeline. The A-pulse and the t-pulse are then read out over a ribbon cable to the 'SVX Sequencer' (originally designed for initialization, control, and readout of SVX IIe silicon vertex detector chips). The differing event sizes anticipated in MICE has required a modification to the Acquire-Digitise-Readout mode structure to be implemented.

### 4.1.1 AFEIIt Firmware

For MICE operation, the AFE-IIt firmware is required to accommodate the expected instantaneous trigger rate of roughly 600 kHz and the time structure of the muon beam. The MICE target is designed to dip into the edge of the ISIS beam for 1 ms at the end of the ramp, just before the beam is extracted. The ISIS proton beam has two 100 ns long bunches that are separated by 200 ns. At the end of the ramp, when the proton-beam energy is 800 MeV, the beam takes 324 ns to make one revolution in the synchrotron. The muon beam for MICE, therefore, appears as a 1 ms wide spill in which two $\sim 100$ ns long bursts of muons arrive at the experiment every 324 ns. The MICE DAQ imposes a trigger constraint such that each L1ACCEPT trigger produces a trigger hold-off of 550 ns so that triggers cannot occur on consecutive bursts (separated by 324 ns). However, since a burst may contain multiple muons and since data from an entire burst will be stored in the TriP-t pipeline, a L1ACCEPT can be associated with multiple muons; the muon rate will be larger than the trigger rate. The timing and spatial separation of multiple muons in a burst will determine whether they can be reconstructed properly. Since this rate is significantly higher than the L1ACCEPT rate in DØ, extensive modifications to the AFE-IIt firmware were required, including modifications to both the digital and analogue data processing (handling of discriminator bits and of the A-pulse and the t-pulse respectively).
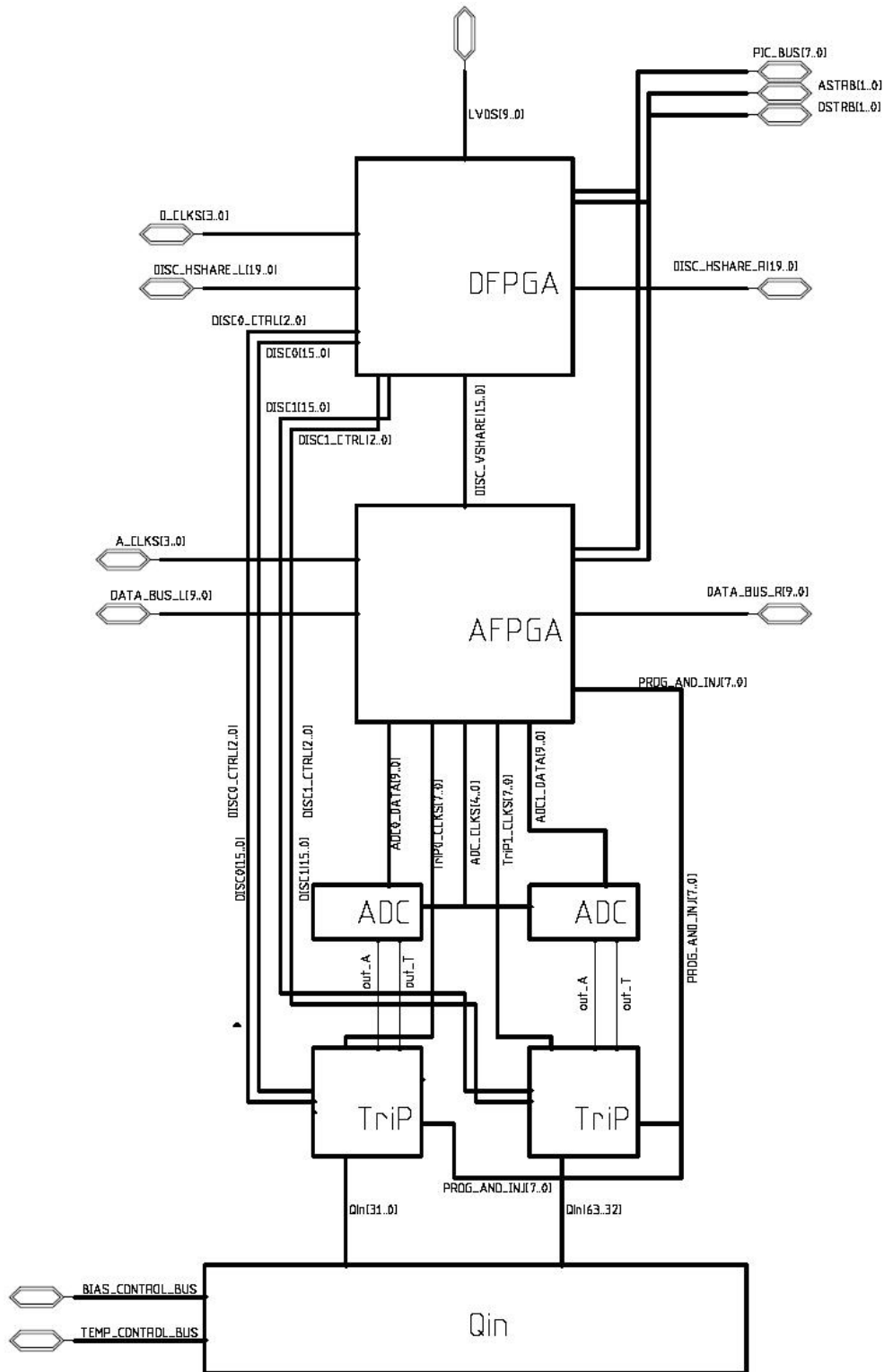
Figure 35: Schematic diagram of the signal path implemented on the AFE-IIt board from the TriP-t chips to the VME memory banks.
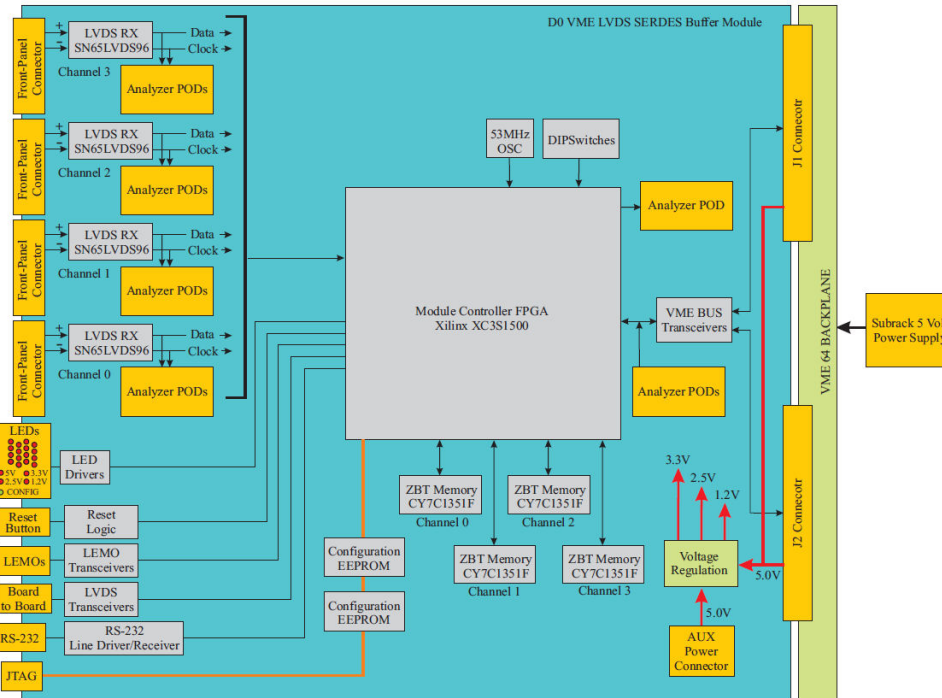
Figure 36: Block diagram of the VLSB board. The diagram shows the module controller, the various blocks of memory and the input/output connections.

## 4.2 VLSB Board

The A-pulse and t-pulse are read out over a Low Voltage Differential Signal (LVDS) path to a custom VME LVDS SERDES (Serializer/Deserializer) Buffer (VLSB) upon receipt of a L1ACCEPT. The VLSB module, which was originally designed for DØ board testing and has been adapted for use in MICE, is a VME64 single width, 6U module. The module is a custom LVDS SERDES buffer with 4 LVDS input channels and can be operated stand-alone. A VLSB module can receive/generate trigger signals over two Lemo connectors on the module front panel. A block diagram of the VLSB card is shown in figure 36 [23].

The module can be controlled through two different interfaces: RS232 (front panel) and VME (backplane). The VLSB module hosts the 'Module Controller FPGA' which handles the VME and RS232 interfaces, the timing and the diagnostics, and supervises the data flow operations. The FPGA is configured at power-up by two on-board EEPROMs. The VLSB module also hosts the four LVDS SERDES receivers used to convert and de-serialize the input LVDS signals to Low Voltage TTL. A logic analyzer pod is provided for each LVDS link. The Module Controller FPGA manages the input LVDS interface and stores the data received into the zero-bus turn-around (ZBT) SRAM. The FPGA control/status registers and the ZBT SRAM content can be accessed from both VME and RS232 interfaces.

In MICE, the L1ACCEPT will be formed from signals from Time-of-Flight counters and signals from the ISIS accelerator; a combination of these signals will indicate the passage of a

through-going muon. If we assume a 0.5% occupancy, then there are roughly 30 hits in the two trackers per muon. During readout, all 64 DFPGAs will read out a trigger word, a header word, and 8 words for bitmap data for a total of 10 words per DFPGA. Then 30 single hits with 5 words per hit (channel, TriP0 time, TriP1 time, TriP0 charge, and TriP1 charge) yield 150 more words for a total of $(64 \times 10) + (30 \times 5) = 790$ total words for a MICE event. Assuming 1000 words/event, then for 600 events/spill and one spill every second, the AFE-IIt boards will have to read out roughly 600,000 words every second to the VLSB buffers via the LVDS links and VME. If the data are read out to 16 VLSB modules housed in two crates with each VME word transfer taking 1 $\mu$s, the 600,000 word readout would take, reading to the two crates in parallel, roughly 0.3 sec which is sufficient for MICE running.

# 5   Performance

## 5.1   Cosmic test stand

The first MICE tracker was installed inside a black carbon fibre cylinder (referred to as the 'coffin') the internal diameter of which is the same as the warm bore of the spectrometer solenoid. The patch panel was connected to the coffin via an aluminium flange and the coffin/patch panel assembly was supported on an aluminium space frame such that the principal axis of the tracker was vertical. Trigger scintillators were placed above and below the tracker and a four-inch layer of lead bricks was placed between the bottom of the tracker and the lower trigger scintillator to filter out muons with momentum less than $\sim 210$ MeV/c. Data taking began in July 2008 and continued without interruption until November 2008 when the cosmic stand was disasembled so that it could be moved to a larger area where both trackers were set up for further testing.

## 5.2   Reconstruction

Reconstruction was performed using the standard routines provided by the G4MICE software package [24]. The principal stages in the track reconstruction are:

- *Cluster finding:*
  Following the unpacking of the hits on individual VLPC channels, clusters of one or two neighbouring channels from a particular view are constructed. Due to the readout arrangement, in which seven neighbouring scintillating fibres are readout via one VLPC channel, a single track can pass through no more than two neighbouring channels. Clusters that have a total reconstructed signal corresponding to at least 2.5 photo-electrons (p.e.) are kept to be used in the reconstruction of space points;

- *Space-point reconstruction:*
  The space-point reconstruction first searches for 'triplets', which consist of a cluster in each of the three views on a given station. If the internal residual, defined as the perpendicular

distance from one cluster to the intersection of the other two, is small enough, and the light yield of each used cluster high enough, the combination of 3 clusters is kept as a space point and the clusters are removed from the list of those available. All combinations of two clusters that have not already been assigned to a point and originate from two different views in the same station are then used to create space points refered to as 'duplets';

- *Pattern recognition and track fit:*
  The pattern recognition code that is used in G4MICE depends on the magnetic field in which the tracker is placed. The cosmic ray test was performed in the absense of a magnetic field and therefore a straight-line track-model is used for the pattern recognition and the track fit.

  Sets of 3 points (in different stations) are tested for collinearity and, if they pass this test, an extrapolation to the remaining two stations is made. If a space point falls inside a small road-width around this extrapolation, then this point is retained. If more than one space point falls inside the road-width for either staion, then the nearest is retained. Each such combination of 5, 4, or 3 points is passed to the Kalman filter track fit [25] and the combination with the smallest $\chi^2$ per degree of freedom is kept. The space points that make up an accepted track are then locked so that they can no longer be used in the track search. The pattern recognition process repeats until no more tracks are found or the list of space points is exhausted.

## 5.3 Performance

The light-yield, space-point-finding efficiency, and the resolution of the tracker were determined using points assigned to tracks by the G4MICE track-finding algorithm described above. The analogue signals produced by the VLPCs are digitised in an ADC with an 8-bit dynamic range. The response of the electronics was calibrated using a light-injection system. The one-, two-, three-, and four-photo-electron peaks were clearly separated from one-another in the calibration data. In addition, the one-photo-electron peak was clearly separated from the pedestal. For each channel, $i$, the calibration data was fitted to extract the pedestal, $p_i$, and the gain $g_i$. For channels in which the ADC value ($\mathrm{ADC}_i$) was below the maximum count of 255, the light yield is given by $l_i = [\mathrm{ADC}_i - p_i]/g_i$. Channels for which $\mathrm{ADC}_i = 255$ are referred to as 'saturated channels'. If the ADC value in all channels that make up a cluster falls below the maximum count, then the cluster light-yield is determined by summing the $l_i$. If a cluster contains one or more saturated channels it is not used in the evaluation of the light yield. To compensate for the saturated channels, the probability of a channel being rejected in this way is calculated as a function of the light-yield, and the initial light-yield distribution divided by this distribution of probabilities. The distribution of the cluster light-yield obtained in this way is shown in figure 37. The mean of the cluster light-yield distribution is $11.23 \pm 0.01$ photo electrons (PE) and the most-probable value is $9.37 \pm 0.03$ PE.

The space-point efficiency was obtained by building tracks using space points in four of the five stations and extrapolating the track to the station under test. If the extrapolated position
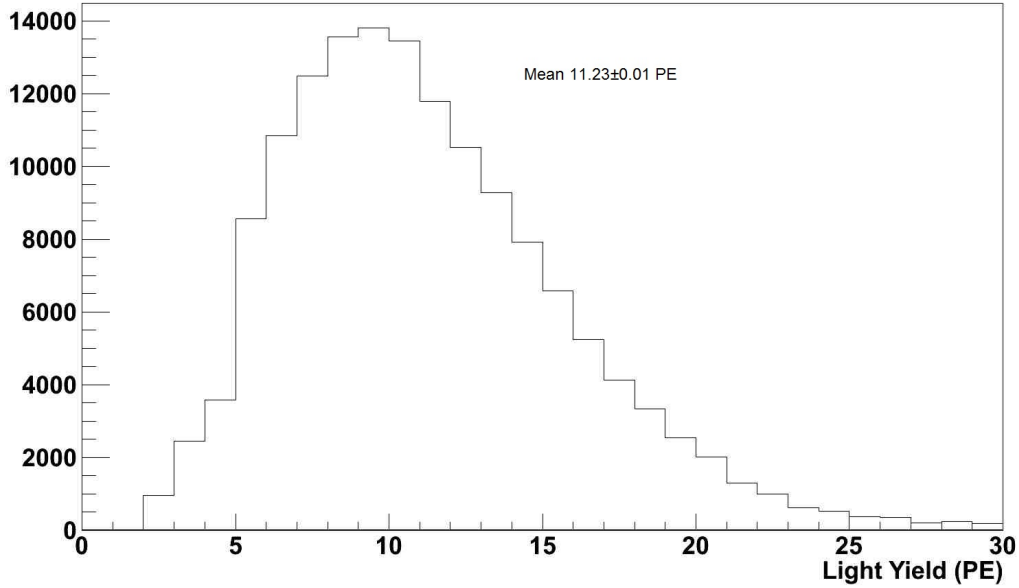
Figure 37: Light yield per doublet cluster from cosmic rays, corrected for saturation effects in high-gain VLPCs.

fell within the active area of the station, a search was made for a space point close to the extrapolated position. Table 3 reports the space-point efficiency determined for each station. The space-point efficiency determined in this way is $99.8 \pm 0.1\%$. The efficiencies are consistent with what would be expected based on the measured light yield reported above.

The intrinsic position resolution of the doublet-layers was evaluated using triplet space points. The construction of the stations is such that the fibres in one view run at an angle of $120°$ with respect to the direction of the fibres in each of the other two views. If $u$, $v$, and $w$ are the position of a cluster in each of the three views that make up the triplet, taking the origin of $u$, $v$, and $w$ to be the centre line of the doublet layer in question, it is expected that the quantity $u + v + w = \delta = 0$. A measure of the intrinsic resolution of a station can therefore be determined by plotting $\delta$. Figure 38a shows the distribution of $\delta$. The width of the distribution of $\delta$ is well described by the Monte Carlo and is as expected from the station construction. To demonstrate that the tracker is precisely aligned and to verify the treatment of material in the track fit, the resolution was determined using reconstructed tracks. Tracks composed of five space points were re-fitted, removing one space point at a time. Each of the five new four-space-point tracks was extrapolated to the station under test and the perpendicular distance (residual) between the extrapolated position and each of the channels forming the removed space point calculated. The distributions of the total residual is shown in figure 38b. The RMS of the residual distributions is $661 \pm 2$ $\mu$m as expected given a channel resolution of $470\mu$m and multiple Coulomb scattering in the doublet layers.
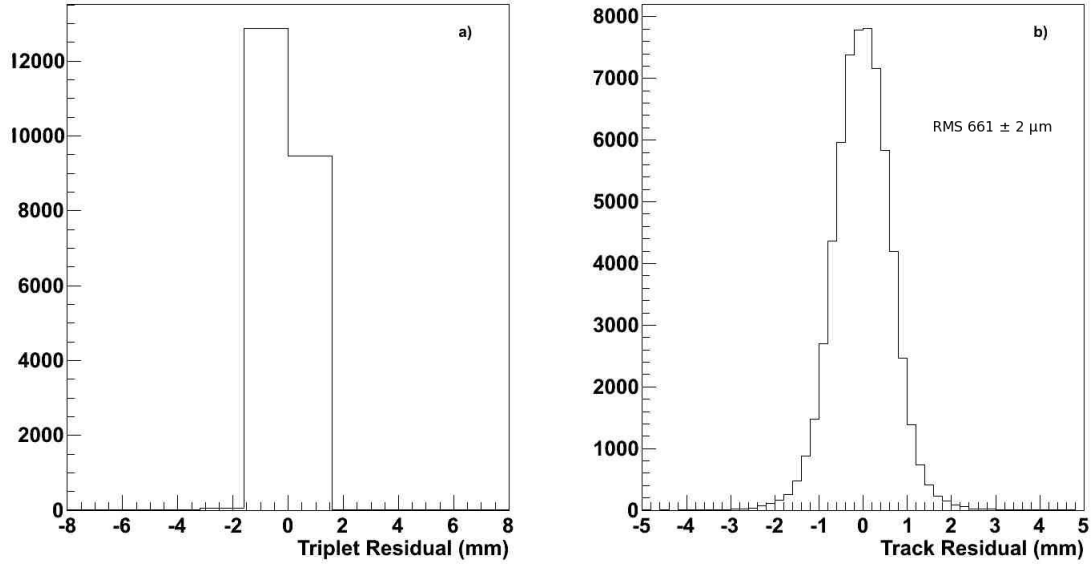
Figure 38: Performance of the MICE tracker evaluated using cosmic rays as described in the text. a) Triplet residual distribution, consisting of triplets made from single-channel clusters and used in full tracks. b) Track residual distribution. The RMS is noted on the figure.

| Station | Efficiency (%) |
|---------|----------------|
| 1 | $99.8 \pm 0.1$ |
| 2 | $99.9 \pm 0.1$ |
| 3 | $99.7 \pm 0.1$ |
| 4 | $99.9 \pm 0.1$ |
| 5 | $99.8 \pm 0.1$ |

Table 3: Efficiency of the five stations that make up the scintillating fibre tracker determined using cosmic rays.

# 6 Summary

The design of the scintillating-fibre trackers for the international Muon Ionisation Cooling Experiment (MICE) which is under construction at the Rutherford Appleton Laboratory has been described. The construction techniques, including the quality assurance procedures, and the optical readout system have been described in detail. Finally, the performance of the first completed device has been presented and shown to meet the design specifications. The two trackers for MICE are presently being commissioned in a cosmic-ray test stand and will be installed in the MICE spectrometer magnets in the near future.

# Acknowledgements

# References

[1] S. Geer, "Neutrino beams from muon storage rings: Characteristics and physics potential," *Phys. Rev.* **D57** (1998) 6989–6997, `hep-ph/9712290`.

[2] D. Neuffer, "Multi-TeV muon colliders," *AIP Conference Proceedings* **156** (1987), no. 1, 201–208.

[3] **MICE** Collaboration, G. Gregoire *et al.*, "An International Muon Ionization Cooling Experiment (MICE)," *MICE Note* **167** (2003) `http://mice.iit.edu/mnp/MICE0021.pdf`.

[4] ISIS Pulsed Neutron & Muon Source. http://www.isis.rl.ac.uk/.

[5] Rutherford Appleton Laboratory (RAL). http://www.scitech.ac.uk/About/find/RAL/introduction.aspx/.

[6] **MICE** Collaboration, "MICE Technical Reference Document - Draft Version." http://www.isis.rl.ac.uk/accelerator/mice/TR/MICE_Tech_Ref.html, 2005.

[7] M. Z. eds. S. Ozaki, R. Palmer and J. Gallardo, "Feasibility Study-II of a Muon-Based Neutrino Source," *BNL-52623* (2001) `www.cap.bnl.gov/mumu/studyii/FS2-report.html`.

[8] J. Birks, *The Theory and Practice of Scintillation Counting*. Pergamon Press, 1964.

[9] C. L. Renschler and L. A. Harrah, "Reduction of Reabsoprtion effects in Scintillators by Employing Solutes with large Stokes Shifts," *Nucl. Instrum. Meth.* **A235** (1985) 41–45.

[10] T. Forster, "Zwischenmolekulare energiewanderung und fluoreszenz," *Naturwissenschaften* **6** (1946) 166–175.

[11] A. Khan *et al.*, "MICE scintillating fibre tracker : First progress report," *MICE Note* **90** (2005) `http://mice.iit.edu/mnp/MICE0090.pdf`.

[12] **DØ** Collaboration, V. M. Abazov *et al.*, "The Upgraded DØ Detector," *Nucl. Instrum. Meth.* **A565** (2006) 463–537, `physics/0507191`.

[13] M. Petroff and M. Stapelbroek, "Photon-Counting Solid-State Photomultiplier," *IEEE TRANSACTIONS ON NUCLEAR SCIENCE* **36** (FEB, 1989) 158–162.

[14] M. Petroff and M. Atac, "High-Energy Particle Tracking using Scintillation Fibers and Solid-State Photomultipliers," *IEEE TRANSACTIONS ON NUCLEAR SCIENCE* **36** (FEB, 1989) 163–164.

[15] P. Rubinov, *AFEIIt Readout Format*, November 2007. DØ Note 5520.

[16] T. M. T. Group, "Specification of the scintillating and clear fibre for the MICE scintillating fibre trackers," (2006) `http://mice.iit.edu/mnp/MICE0135.pdf`.

[17] P. K. M. Takahashi, P.R. Hobson and J. Nebrensky, "Illumination System for the MICE Tracker Station Assembly QA," *MICE Note* **167** (2007) http://mice.iit.edu/micenotes/public/pdf/MICE0167/MICE0167.pdf.

[18] ZEMAX Development Corporation, 3001 112th Avenue NE, Suite 202, Bellevue, WA 98004-8017 USA. http://www.zemax.com/.

[19] Kuraray Company Ltd. Otemachi, Chiyoda-ku, Tokyo 100-8115, Japan, http://www.kuraray.co.jp/en/company/.

[20] A. Bross, E. Flattum, D. Lincoln, S. Gruenendahl, J. Warchol, M. Wayne, and P. Padley, "Characterization and performance of visible light photon counters (VLPCs) for the upgraded DØdetector at the Fermilab Tevatron," *Nuclear Instruments and Methods in Physics Research Section A: Accelerators, Spectrometers, Detectors and Associated Equipment* **477** (2002), no. 1-3, 172 – 178.

[21] RDK-415D cryocooler from Sumitomo Heavy Industries Ltd. http://www.shicryogenics.com/language.jssx.

[22] Lakeshore Cryogenics, www.lakeshore.com.

[23] S. Rapisarda *et al.*, *VME LVDS SERDES Buffer (VLSB) Module Specification*, February 2005. ESE--041101.

[24] M. Ellis, "MICE Software Design and Physics Performance," *Proceedings of the 10th ICATPP Conference on Astroparticle, Particle and Space Physics, Detectors and Medical Physics Applications* (2008) 763–770.

[25] A. Cervera-Villanueva, J. J. Gomez-Cadenas, and J. A. Hernando, "RecPack: A reconstruction toolkit," *Nucl. Instrum. Meth.* **A534** (2004) 180–183.

[26] **MICE** Collaboration, P. Gruber and E. McKigney, "A first study of a scintillating fibre detector for a muon ionisation cooling experiment," *CERN Neutrino Factory Note* **79** (2001) http://slap.web.cern.ch/slap/NuFact/NuFact/nf79.pdf.

[27] **MICE** Collaboration, P. Gruber and E. McKigney, "A first study of a scintillating fibre detector for a muon ionisation cooling experiment," *CERN Neutrino Factory Note* **79** (2001) http://www.imperial.ac.uk/research/hep/preprints/01-1.pdf.

[28] P. Janot. Workshop on a Muon Ionization Cooling Experiment, CERN, 25-27 October 2001. http://muonstoragerings.web.cern.ch/muonstoragerings/October01WS/mucool.ppt.